Electronic Supplementary Information

Synergy of redox-activity and hemilability in thioamidato cobalt(III) complexes for the chemoselective reduction of nitroarenes to anilines: catalytic and mechanistic investigation

Dimitra K. Gioftsidou,[a] Michael G. Kallitsakis,[a] Konstantina Kavaratzi,[a] Antonios G. Hatzidimitriou,[a] Michael A. Terzidis,[b] Ioannis N. Lykakis[a,*] and Panagiotis A. Angaridis[a,*]

[a] *Laboratory of Inorganic Chemistry, Department of Chemistry, Aristotle University of Thessaloniki, 54124 Thessaloniki, Greece*
[b] *Laboratory of Organic Chemistry, Department of Chemistry, Aristotle University of Thessaloniki, 54124 Thessaloniki, Greece*
[c] *Department of Nutrition Sciences and Dietetics, International Hellenic University, Sindos, 57400 Thessaloniki, Greece*

Table of Contents

S1 EXPERIMENTAL

S1.1 General procedures and chemicals

All manipulations were carried out under atmospheric conditions. Solvents were purified according to established methods and allowed to stand over molecular sieves for 24 h. 2-mercaptopyrimidine (pymtH), 4,6-dimethyl-2-pyrimidinethiol (dmp2SH), 4,6-diamino-2-pyrimidinethiol (damp2SH), 2-mercaptopyridine (2-mpyH), triphenylphosphine (PPh_3), 1,2-bis(diphenylphosphino)ethane (dppe), pyridine (py), diethylamine ($(CH_3CH_2)_2NH$), sodium methoxide (CH_3ONa), ammonium hexafluorophosphate (NH_4PF_6), tetraethylammonium hexafluorophosphate ($(CH_3CH_2)_4NPF_6$), [$CoCl_2{\cdot}6H_2O$] and [$Co(acac)_3$], as well as methylhydrazine (CH_3NHNH_2), nitroarenes, nitrosobenzenes, nitroalkane, nitroalkene were obtained from commercial sources and used without any further purification.

S1.2 Syntheses

General synthesis of [Co(L^NS)$_3$] (1-4 and 6). $CoCl_2{\cdot}6H_2O$ (0.119 g, 0.5 mmol) was dissolved in 15 mL of CH_3OH. Alongside, to a methanol solution (15 mL) of the corresponding heterocyclic thioamide $L^{NH}S$ (1.5 mmol), $(CH_3CH_2)_2NH$ (1.5 mmol) was added dropwise. The resulting solution of the deprotonated heterocyclic thioamidate (L^NS^-) was stirred at room temperature for 30 min and then it was added slowly to the Co-containing solution. The reaction mixture was stirred at 60-70°C for 3 h. After filtration, the dark brown filtrate was set aside to evaporate slowly at room temperature and, over a period of a few days, crystals of **1**-**4** and **6** were formed.

[Co(pymt)$_3$] (1). Dark brown crystals. Yield (based on Co): 58%. Anal. for $C_{14}H_{12}CoN_7S_3$: Calcd (%) C, 38.80; H, 2.79; N, 22.62. Found (%) C, 38.90; H, 2.95; N, 22.75. FTIR (KBr, cm^{-1}): 3446(w br), 1560(m), 1544(m), 1426(w), 1369(s), 1241(w br), 1201(w), 1168(w), 1095(w), 1061(w), 1010(w), 797(w br), 753(m), 665(w), 4809(w br). UV-vis (CH_3OH), λ_{max}/nm ($\varepsilon/M^{-1}\,cm^{-1}$): 315 (7568), 630 (119). ^{1}H NMR (500 MHz, $CDCl_3$): δ (ppm) 8.61 (s, 1 H), 8.41-8.37 (d, 4 H), 7.43 (s, 2 H), 7.11 (s, 1 H), 6.79 (s, 1 H). $^{13}C\{^1H\}$ NMR (125 MHz, $CDCl_3$): δ (ppm) 187.42, 186.49, 185.38, 169.74, 158.55, 158.31, 157.94, 157.48, 155.36.

[Co(tfmp2S)$_3$] (2). Recrystallization from CH_2Cl_2/hexane. Brown crystals. Yield (based on Co): 70%. Anal. for $C_{15}H_6CoF_9N_6S_3{\cdot}0.16CH_2Cl_2$: Calcd. (%) C, 29.84; H, 1.05; N, 13.77. Found (%) C, 30.07; H, 1.26; N, 13.53. FTIR (KBr, cm^{-1}): 3415(m br), 1637(w), 1617(w), 1572(s), 1555(s), 1421(m), 1364(s), 1328(s), 1194(s br), 1150(s br), 1112(s), 1018(w), 1010(w), 834(m), 831(m), 736(m), 688(m), 618(w br), 525(w), 485(w). UV-vis (CH_3OH), λ_{max}/nm ($\varepsilon/M^{-1}\,cm^{-1}$): 323 (15469), 640 (163). ^{1}H NMR (500 MHz, $CDCl_3$): δ (ppm) 8.64 (s, 1 H), 8.60 (s, 1 H), 7.74 (s, 1 H), 7.22 (s, 1H), 7.09 (s, 1 H), 6.98 (s, 1 H). $^{13}C\{^1H\}$ NMR (125 MHz, $CDCl_3$): δ (ppm) 187.3, 185.6, 185.0, 161.0, 159.9, 158.0, 157.8, 157.5, 157.1, 119.09, 119.06, 119.0, 111.0, 110.7, 109.9.

[Co(dmp2S)$_3$] (3). Dark green crystals. Yield (based on Co): 65%. Anal. for $C_{19}H_{22.5}CoN_{6.5}S_3$: Calcd. (%) C, 46.41; H, 4.67; N, 18.94. Found (%) C, 46.51; H, 4.59; N, 18.86. FTIR (KBr, cm^{-1}): 3480(wbr), 1580(s), 1525(s), 1430(sbr), 1353(w), 1338(m), 1267(s), 1194(w), 1174(m), 1027(w), 1001(w), 925(m), 889(w), 844(m), 578(mbr). UV-vis (CH_3OH), λ_{max}/nm ($\varepsilon/M^{-1}\,cm^{-1}$): 322 (12324), 614 (94). ^{1}H NMR (500 MHz, $CDCl_3$): δ (ppm) 6.42 (s, 3 H), 2.42 (s, 9 H), 1.78 (s, 9 H). $^{13}C\{^1H\}$ NMR (125 MHz, $CDCl_3$): δ (ppm) 185.83, 185.79, 185.75, 168.35, 166.77, 115.18, 24.07, 19.97.

[Co(damp2S)$_3$] (4). Brown crystals. Yield (based on Co): 68%. Anal. for $C_{13.3}H_{20}CoN_{12}O_{1.4}S_3$: Calcd. (%) C, 31.14; H, 4.70; N, 29.05. Found (%) C, 31.26; H, 4.58; N, 29.15. FTIR (KBr, cm^{-1}): 3301(m br), 3138(m br), 1624(s), 1573(s), 1533(s), 1470(s), 1319(m), 1276(m), 1253(m br), 1043(w), 995(w), 937(w), 795(w), 589(w). UV-vis (CH_3OH), λ_{max}/nm (ε/M^{-1} cm^{-1}): 309 (10680), 640 (189). NMR data couldn't be obtained due to its very low solubility.

[Co(2-mpy)$_3$] (6). Recrystallization from CH_2Cl_2/hexane. Brown crystals. Yield (based on Co): 85%. Anal. for $C_{15}H_{12}CoN_3S_3$: Calcd. (%) C, 46.27; H, 3.11; N, 10.79. Found (%) C, 46.35; H, 3.19; N, 10.86. FTIR (KBr, cm^{-1}): 1576(m), 1552(w), 1439(m), 1422(m), 1254(m), 1138(m), 1087(w), 1025(w), 750(m), 732(m), 658(w), 495(w). UV-vis (CH_3OH), λ_{max}/nm (ε/M^{-1} cm^{-1}): 322 (10624), 650 (122). ^{1}H NMR (500 MHz, $CDCl_3$): δ (ppm) 9.57 (s, 1 H), 8.28 (s, 1 H), 7.50-7.47 (t, 1 H), 7.42-7.38 (t, 2 H),7.08 (s, 1 H), 6.83-6.78 (m, 4 H), 6.69-6.67 (t, 1 H), 6.60-6.57 (t, 1 H). ^{13}C{^{1}H} NMR (125 MHz, CD_3COCD_3): δ (ppm) 178.63, 178.50, 178.44, 150.32, 149.62, 148.40, 137.29, 136.83, 136.63, 136.00, 135.74, 125.80, 124.47, 117.49, 116.72.

[Co(pymt)$_3$(PPh$_3$)] (5). 0.119 g (0.5 mmol) of $CoCl_2{\cdot}6H_2O$ was dissolved in 20 mL of CH_3OH. An amount of 0.113 g (1 mmol) of pymtH was dissolved in 10 mL of CH_3OH and then 4.2 mL of KOH 0.24 M (1 mmol) was added. The dark yellow solution was stirred for 20 min and then 0.265 g (1.0 mmol) of PPh_3 added. The resulting solution was added to the Co-containing solution. The reaction mixture was stirred at 50°C for 2 h and then it was filtered. The brown filtrate was allowed to evaporate slowly leading to the precipitation of dark brown crystals of compound **5** within 7 days. Yield (based on Co): 82%. Anal. for $C_{30}H_{24}CoN_6PS_3$: Calcd. (%) C, 55.04; H, 3.70; N, 12.84. Found (%) C, 55.14; H, 3.82; N, 12.72. FTIR (KBr, cm^{-1}): 1558(w), 1542(w), 1430(v w), 1378(m), 1253(v w), 1094(v w), 755(w), 699(w), 500(v w). UV-vis (CH_3OH), λ_{max}/nm (ε/M^{-1} cm^{-1}): 306 (2927), 640 (100). ^{1}H NMR (500 MHz, $CDCl_3$): δ (ppm) 8.81-8.77 (d, 1 H), 8.62 (s, 1 H), 7.77 (t br, 6 H), 7.67 (t br, 2 H), 7.54-7.53 (t, 1 H), 7.47 (t, 3 H), 7.37 (m, 3 H), 7.28 (m br, 5 H), 7.16 (s br, 1 H), 6.84 (s br, 1 H). ^{13}C{^{1}H} NMR (125 MHz, $CDCl_3$): δ (ppm) 179.93, 179.81, 171.80, 158.38, 155.32, 153.13, 134.01, 133.54, 133.47, 131.94, 131.59, 128.45, 128.25, 128.21, 128.17, 128.13, 116.32.

[Co(2-mpy)$_2$(dppe)]PF$_6$ (7). 0.119 g of $CoCl_2{\cdot}6H_2O$ (0.5 mmol) was added in 30 mL of CH_3OH. 0.111 g (1 mmol) 2-mpyH and 0.199 g dppe (0.5 mmol) were added in 15 mL CH_3OH. After stirring 0.07 mL of $(CH_3CH_2)_2NH$ (0.7 mmol) was added. Then the dark yellow solution was added to the Co-containing solution and the total solution was stirred for 1 h at 60 °C. After cooling, the solution was filtered and 0.138 g of NH_4PF_6 (0.5 mmol) was added to the brown filtrate. The total solution was stirred for 30 min and then the brown-green filtrate was allowed to evaporate slowly. After 7 days, brown-greenish crystals were obtained. Yield (based on Co): 80%. Anal. for $C_{36}H_{32}CoF_6N_2O_{0.25}P_3S_2$: Calcd. (%) C, 52.95; H, 4.79; N, 3.17. Found (%) C, 52.80; H, 4.84; N, 3.25. FTIR (KBr, cm^{-1}): 3439(m br), 1631(w), 1581(m), 1551(w), 1485(w), 1435(m br), 1425(m), 1260(m), 1190(w), 1137(m), 1094(m), 1024(w), 999(w), 840(s), 747(m br), 732(m br), 688(m br), 591(w), 557(m), 533(m), 492(w). UV-vis (CH_3OH), λ_{max}/nm (ε/M^{-1} cm^{-1}): 315 (15741), 610 (185). ^{1}H NMR (500 MHz, CD_3CN): δ (ppm) 8.39-8.38 (d, 2 H), 7.69-7.63 (m, 6 H), 7.60-7.58 (t, 4 H), 7.45-7.43 (t, 2 H), 7.39-7.38 (t, 2 H), 7.18-7.16 (m, 8 H), 7.00-6.99 (t, 2 H), 6.42-6.40 (d, 2 H), 1.32-1.29 (t, 4 H). ^{13}C{^{1}H} NMR (126 MHz, CD_3CN): δ (ppm) 175.21, 147.50, 137.88, 131.78, 129.23, 128.09, 125.57, 119.62, 23.03.

[Co(2-mpy)$_2$(py)$_2$]PF$_6$ (8). 0.238 g of $CoCl_2{\cdot}6H_2O$ (1 mmol) was added in 40 mL CH_3OH. 0.222 g (2 mmol) of 2-mpyH and 0.32 mL (1 mmol) of py dissolved in 10 mL of CH_3OH and then was added 0.068 g of CH_3ONa (1.25 mmol). After 15 min the deprotonation solution was added to the Co-containing solution and the total dark brown solution was stirred for 15 min. Filtration was followed and 0.275 g $(CH_3CH_2)_4NPF_6$ (1 mmol) dissolved in 5 mL CH_3OH. The total solution was stirred and the brown filtrate was allowed to crystallize by slow evaporation at room temperature. After a week

brown crystal were received. Yield (based on Co): 77%. Anal. for $C_{20}H_{18}CoF_6N_4PS_2$: Calcd. (%) C, 44.09; H, 4.18; N, 8.94. Found (%) C, 44.18; H, 4.23; N, 8.89. FTIR (KBr, cm^{-1}): 1606(w br), 1579(m br), 1554(w), 1488(w), 1443(m), 1422(m), 1358(w), 1266(m), 1220(w), 1154(w), 1140(m), 1092(w), 1070(m), 877(w), 840(s), 758(m), 734(w), 697(m), 557(m), 468(w). UV-vis (CH_3OH), λ_{max}/nm (ε/M^{-1} cm^{-1}): 323 (16241), 650 (214). ^1H NMR (500 MHz, $CDCl_3$): δ (ppm) 8.27 (s br, 4 H), 7.50-7.47 (t, 2 H), 7.40 (t br, 2 H), 7.07 (s br, 2 H), 6.83-6.78 (q, 6 H), 6.68 (t, 1 H), 6.58 (t, 1 H). $^{13}C\{^1H\}$ NMR (126 MHz, CD_3COCD_3): δ (ppm) 178.75, 178.26, 150.21, 149.61, 147.56, 137.30, 136.63, 136.00, 125.51, 125.39, 125.14, 117.61, 116.99.

S1.3 Instrumentation

Elemental analyses were obtained on a PerkinElmer 240B elemental microanalyzer. Infra-red spectra were recorded on a Nicolet FT-IR 6700 spectrophotometer as KBr discs in the region of 4000-400 cm^{-1}. UV-vis electronic absorption spectra were obtained on a Shimadzu 160A spectrophotometer as 1.0×10^{-3} M and 1.0×10^{-4} M solutions in CH_3OH. Cyclic voltammetry measurements were conducted on an Autolab electrochemical analyzer, using a carbon working electrode, a platinum counter electrode, and an Ag/AgCl electrode saturated with a KCl reference electrode in 8 mL of CH_3OH or CH_3CN solutions with 0.1 M Bu_4NBF_4 as supporting electrolyte, and a scan rate of 0.1 V s^{-1}. Argon was used to purge all samples. In the acetic acid concentration dependence study, a stock solution of CH_3COOH (8.56 M) was prepared in CH_3CN. To a stirred and degassed 1.0 mM catalyst solution, 4-20 mM of acid stock solution was added and purged with argon for 120 s before performing cyclic voltammetry. ^{1}H and $^{13}C\{^{1}H\}$ NMR spectra were recorded in $CDCl_3$, CD_3CN, CD_3OD and CD_3COCD_3 solutions on an Agilent 500 MHz spectrometer. Chemical shifts were reported as δ values using the solvent as internal standard.

S1.4 Single crystal X-ray diffraction analysis

Single crystals of all compounds, suitable for X-ray diffraction analysis, were mounted on thin glass fibers with the aid of an epoxy resin. X-ray diffraction data were collected on a Bruker Apex II CCD area-detector diffractometer, equipped with a Mo Ka (λ = 0.71070 Å) sealed tube source, at 295 K, using the ϕ and ω scans technique. The program Apex2 (Bruker AXS, 2006) was used in data collection, cell refinement, and data reduction.[1] Structures were solved and refined with full-matrix least-squares using the program Crystals.[2] Anisotropic displacement parameters were applied to all non-hydrogen atoms, while hydrogen atoms were generated geometrically and refined using a riding model. Details of crystal data and structure refinement parameters are shown in Table S1. Plots of the molecular structures of all compounds were obtained by using Mercury software.[3]

S1.5 Catalytic reactions

Evaluation of catalytic activity of complexes 1-8. To a sealed tube containing 4-nitrotoluene (0.2 mmol) and 1 mL CH_3OH were added 5 equiv of CH_3NHNH_2 (1 mmol) and the respective catalyst **1**-**8** (1-2 mol %). The reaction was heated at 70 °C for 4 h. The reaction was monitored by TLC, and after completion the solvent was evaporated under vacuum, small amount of ethyl acetate was added, and the slurry was filtered under pressure through a short pad of silica gel to withhold the catalyst. The filtrate was evaporated under vacuum to afford the corresponding amine in almost pure form.

Application of catalytic reaction to substrates 1a-17a. Analogous reactions, under similar experimental conditions, were conducted for substrates **1a**-**17a** using complex **2** as catalyst. Spectroscopic data (^1H and $^{13}C\{^1H\}$ NMR) of the products of the reactions are in agreement with those reported in the literature.[4,5,6]

S2 RESULTS AND DISCUSSION

S2.1 Single-crystal X-ray diffraction analysis

Table S1. Crystal data, data collection and refinement parameters for complexes **1**, **3**, **4**, **5**, **7** and **8**.

	1·2CH_3CN	**3**·0.5CH_3CN	**4**·1.25CH_3OH
CCDC Deposition Number	1995929	1995931	1995932
Chemical formula	$C_{12}H_9CoN_6S_3$	$C_{18}H_{21}CoN_6S_3$	$C_{12}H_{15}CoN_{12}S_3$
Formula weight	433.43	497.06	522.52
Crystal system	Orthorhombic	Orthorhombic	Monoclinic
Space group	*Pbcb*	*P*na2_1	*P*2_1/*c*
Temperature (K)	295	295	295
Unit cell parameters			
a (Å)	10.3110 (17)	15.4562 (8)	10.7282 (13)
b (Å)	12.3024 (19)	19.4479 (14)	29.457 (3)
c (Å)	28.363 (6)	8.1889 (4)	8.1158 (8)
Volume (Å^3)	3597.8 (11)	2461.5 (2)	2503.1 (5)
Z	8	4	4
Radiation type, λ (Å)	Mo Kα	Mo Kα	Mo Kα
Absorption coefficient (mm^{-1})	1.31	0.97	0.97
Crystal size (mm)	0.14 × 0.12 × 0.07	0.19 × 0.17 × 0.13	0.20 × 0.19 × 0.14
Diffractometer	Bruker Kappa Apex2	Bruker Kappa Apex2	Bruker Kappa Apex2
Absorption correction	Numerical Analytical Absorption (De Meulenaer & Tompa, 1965)	Numerical Analytical Absorption (De Meulenaer & Tompa, 1965)	Numerical Analytical Absorption (De Meulenaer & Tompa, 1965)
T_{min}, T_{max}	0.85, 0.91	0.85, 0.88	
Number of measured, independent and observed [I> 2.0σ(I)] reflections	26550, 3452, 2906	15406, 4989, 3258	41557, 4814, 3903
Rint	0.028	0.022	0.040
(sin θ/λ)$_{max}$ (Å^{-1})	0.612	0.626	0.617
R[F^2>2σ(F^2)], wR(F^2), S	0.047, 0.070, 1.00	0.023, 0.049, 1.00	0.045, 0.070, 1.00
No. of reflections	2906	3258	3903
No. of parameters	228	266	277
Δρ$_{max}$, Δρ$_{min}$ (e Å^{-3})	0.65, −0.34	0.24, −0.22	0.39, −0.38

(continued)

(continued)

	5	**7**·0.25H_2O	8
CCDC Deposition Number	1995933	1995934	1995935
Chemical formula	$C_{30}H_{24}CoN_6PS_3$	$C_{36}H_{32}CoF_6N_2O_{0.25}P_3S_2$	$C_{20}H_{18}CoF_6N_4PS_2$
Formula weight	654.67	826.64	582.42
Crystal system	Triclinic	Orthorhombic	Monoclinic
Space group	*P*-1	$P2_12_12_1$	$P2_1/c$
Temperature (K)	295	295	295
Unit cell parameters			
a (Å)	10.1905 (15)	12.6502 (5)	8.7104 (12)
b (Å)	11.2851 (16)	13.2027 (5)	20.042 (3)
c (Å)	14.0183 (19)	22.5410 (8)	13.7941 (17)
Volume (Å^3)	1452.2 (6)	3764.7 (2)	2408.0 (6)
Z	2	4	4
Radiation type, λ (Å)	Mo Kα	Mo Kα	Mo Kα
Absorption coefficient (mm^{-1})	0.89	0.75	1.01
Crystal size (mm)	0.23 × 0.16 × 0.07	0.20 × 0.17 × 0.11	0.26 × 0.19 × 0.17
Diffractometer	Bruker Kappa Apex2	Bruker Kappa Apex2	Bruker Kappa Apex2
Absorption correction	Numerical Analytical Absorption (De Meulenaer & Tompa, 1965)	Numerical Analytical Absorption (De Meulenaer & Tompa, 1965)	Numerical Analytical Absorption (De Meulenaer & Tompa, 1965)
T_{min}, T_{max}	0.87, 0.94	0.88, 0.92	0.82, 0.84
Number of measured, independent and observed [I> 2.0σ(I)] reflections	37275, 5409, 3985	24737, 7688, 5868	43635, 5311, 4513
Rint	0.052	0.016	0.028
$(\sin\theta/\lambda)_{max}$ (Å^{-1})	0.617	0.626	0.643
R[F^2>2σ(F^2)], wR(F^2), S	0.040, 0.072, 1.00	0.031, 0.052, 1.00	0.066, 0.131, 1.00
No. of reflections	3985	5868	4513
No. of parameters	370	456	301
$\Delta\rho_{max}$, $\Delta\rho_{min}$ (e Å^{-3})	0.40, −0.36	0.33, −0.72	1.12, −0.67

Table S2. Bond distances (Å) and angles (deg) of **1**-**4**.

	1	2[a]	3	4
		bond distances (Å)		
Co–N	1.900 (2)	1.911 (5)	1.962 (2)	1.946 (2)
	1.918 (2)	1.924 (6)	1.968 (2)	1.959 (2)
	1.945 (3)	1.927 (6)	1.986 (2)	1.971 (2)
Co–S	2.283 (9)	2.250 (2)	2.249 (9)	2.269 (1)
	2.293 (9)	2.275 (2)	2.256 (9)	2.291 (9)
	2.319 (9)	2.306 (2)	2.265 (9)	2.301 (9)
		bond angles (deg)		
$N–Co–S_{cis}$	72.98 (7), 93.72 (8)	72.42 (16), 94.39 (18)	72.60 (7), 91.64 (7)	72.32 (7), 96.56 (7)
	72.91 (7), 95.30 (7)	72.42 (18), 95.92 (18)	73.23 (8), 90.09 (7)	71.70 (7), 90.95 (7)
	72.16 (8), 99.59 (8)	72.79 (18), 96.2 (2)	72.18 (7), 91.51 (7)	71.86 (7), 97.06 (8)
$N–Co–S_{trans}$	94.64 (7)	96.61 (17)	166.36 (8)	101.45 (7)
	100.20 (8)	99.05 (18)	167.53 (8)	101.34 (8)
	166.68 (8)	166.86 (18)	167.20 (8)	163.72 (7)
$N–Co–N_{cis}$	93.05 (10)	93.7 (3)	100.94 (10)	94.27 (11)
	95.76 (11)	99.4 (2)	101.56 (11)	99.03 (10)
$N–Co–N_{trans}$	169.31 (10)	162.5 (2)	102.12 (10)	164.21 (10)
$S–Co–S_{cis}$	92.44 (3)	94.55 (8)	94.49 (3)	93.13 (4)
	101.61 (4)	97.49 (8)	95.82 (3)	94.55 (3)
$S–Co–S_{trans}$	162.72 (4)	166.03 (9)	96.37 (3)	170.62 (3)

[a]Data are given for only one of the three symmetry independent molecules of the asymmetric unit of the crystallographic unit cell.

Table S3. Bond distances (Å) and angles (deg) of **5**.

bond distances (Å)					
Co1–P1	2.270 (2)	Co1–N3	1.957 (3)	Co1–S2	2.335 (1)
Co1–N1	1.950 (3)	Co1–S1	2.307 (1)	Co1–S3	2.287 (1)
bond angles (deg)					
P1–Co1–S1	100.23 (5)	S2–Co1–S3	166.60 (4)	S3–Co1–N1	93.68 (11)
P1–Co1–S2	91.60 (5)	P1–Co1–N1	172.42 (9)	S1–Co1–N3	161.97 (9)
P1–Co1–S3	86.32 (5)	P1–Co1–N3	94.40 (10)	S2–Co1–N3	71.40 (10)
S1–Co1–S2	97.54 (6)	S1–Co1–N1	72.22 (10)	S3–Co1–N3	95.54 (10)
S1–Co1–S3	95.85 (6)	S2–Co1–N1	90.11 (10)	N1–Co1–N3	93.15 (12)

Table S4. Bond distances (Å) and angles (deg) of **7** and **8**.

7				8			
bond distances (Å)							
Co1–S1	2.284 (1)	Co1–N2	1.967 (2)	Co1–S1	2.291 (1)	Co1–N2	1.932 (3)
Co1–S2	2.292 (1)	Co1–P1	2.227 (1)	Co1–S2	2.317 (1)	Co1–N3	1.951 (4)
Co1–N1	1.962 (2)	Co1–P2	2.222 (1)	Co1–N1	1.923 (3)	Co1–N4	1.961 (3)
bond angles (deg)							
P1–Co1–P2	87.38 (3)	S1–Co1–S2	165.70 (4)	S1–Co1–N1	72.23 (10)	S1–Co1–S2	162.71 (5)
P1–Co1–S1	101.16 (3)	S1–Co1–N1	72.41 (8)	S2–Co1–N1	95.31 (10)	N1–Co1–N2	87.99 (14)
P2–Co1–S1	90.39 (3)	S2–Co1–N1	96.72 (8)	S1–Co1–N2	95.16 (10)	N1–Co1–N3	170.74 (15)
P1–Co1–S2	89.44 (3)	S1–Co1–N2	97.22 (7)	S2–Co1–N2	71.96 (10)	N1–Co1–N4	92.19 (13)
P2–Co1–S2	99.75 (3)	S2–Co1–N2	72.60 (7)	S1–Co1–N3	98.81 (11)	N2–Co1–N3	90.54 (14)
P1–Co1–N1	173.47 (8)	P1–Co1–N2	92.02 (7)	S2–Co1–N3	92.92 (11)	N2–Co1–N4	171.31 (14)
P2–Co1–N1	93.68 (7)	P2–Co1–N2	172.34 (7)	S1–Co1–N4	93.16 (10)	N3–Co1–N4	90.64 (14)
N1–Co1–N2	87.79 (9)			S2–Co1–N4	99.39 (10)		

S2.2 ^{1}H and ^{13}C{H} NMR spectra of Co(III) complexes

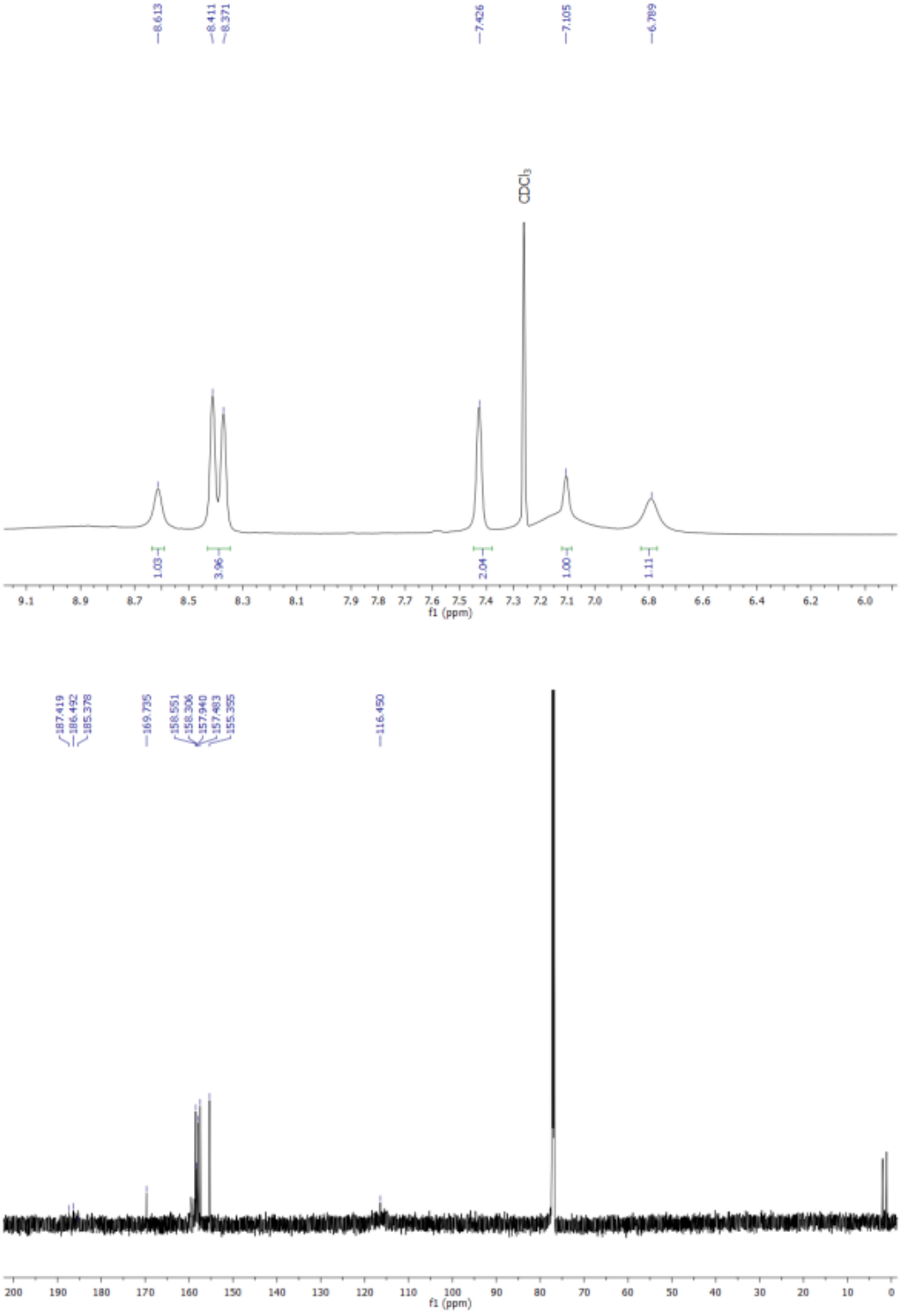

Figure S1. ^{1}H NMR (500 MHz, $CDCl_3$) and ^{13}C{H} NMR (125 MHz, $CDCl_3$) spectra of **1**.

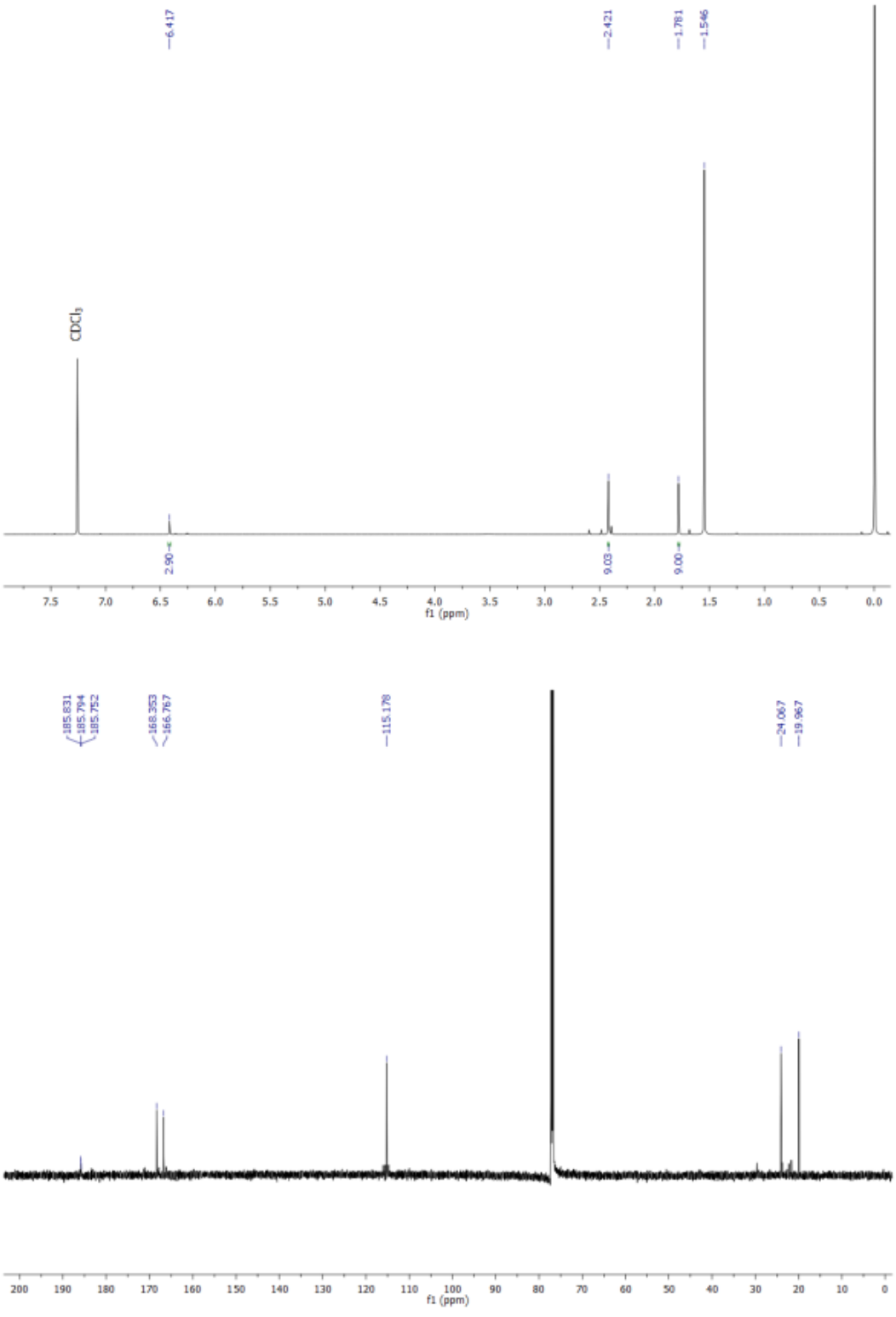

Figure S2. ^{1}H NMR (500 MHz, $CDCl_3$) and $^{13}C\{H\}$ NMR (125 MHz, $CDCl_3$) spectra of **3**.

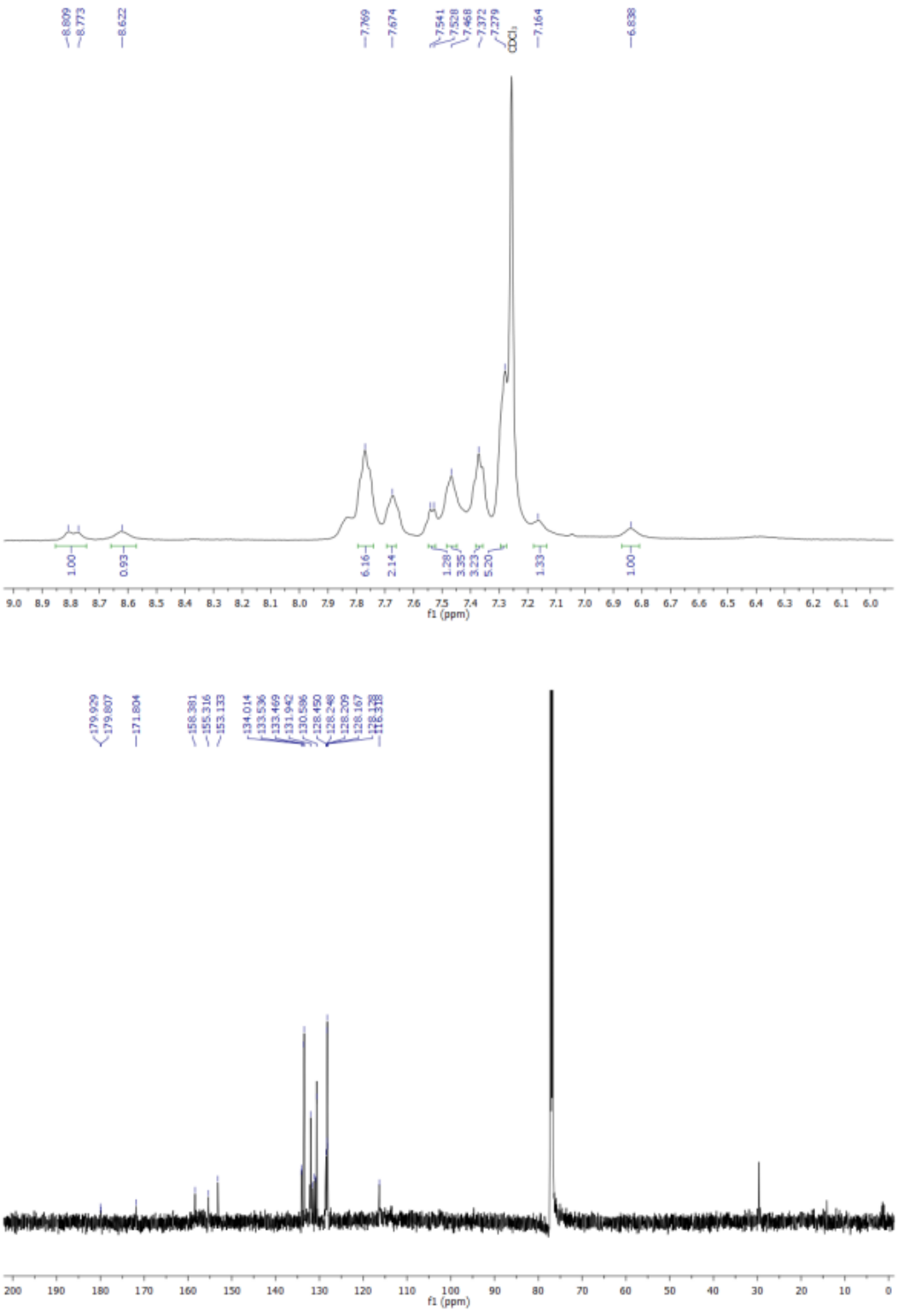

Figure S3. ^{1}H NMR (500 MHz, $CDCl_3$) and $^{13}C\{H\}$ NMR (125 MHz, $CDCl_3$) spectra of **5**.

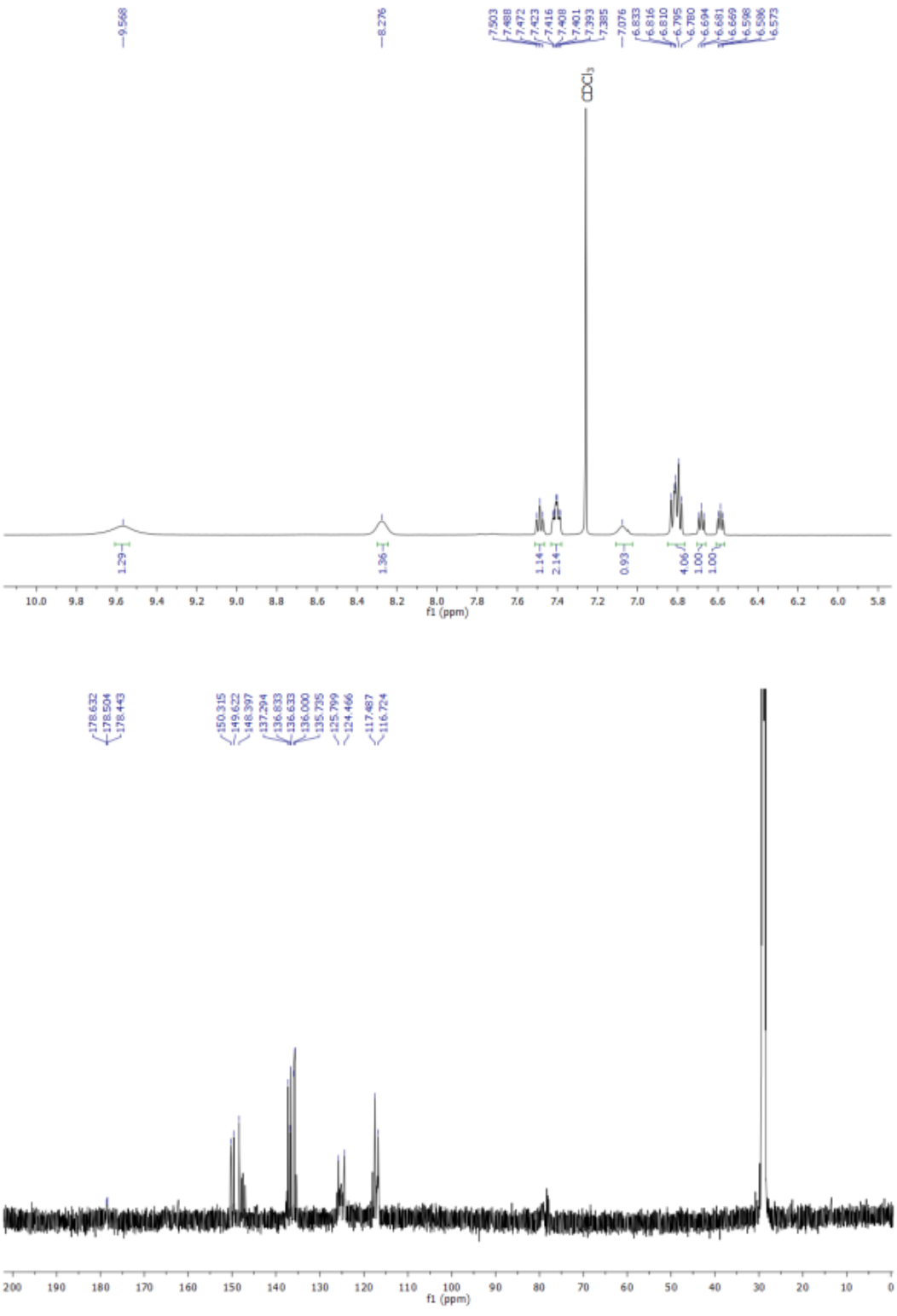

Figure S4. ^{1}H NMR (500 MHz, $CDCl_3$) and $^{13}C\{H\}$ NMR (125 MHz, $CDCl_3$) spectra of **6**.

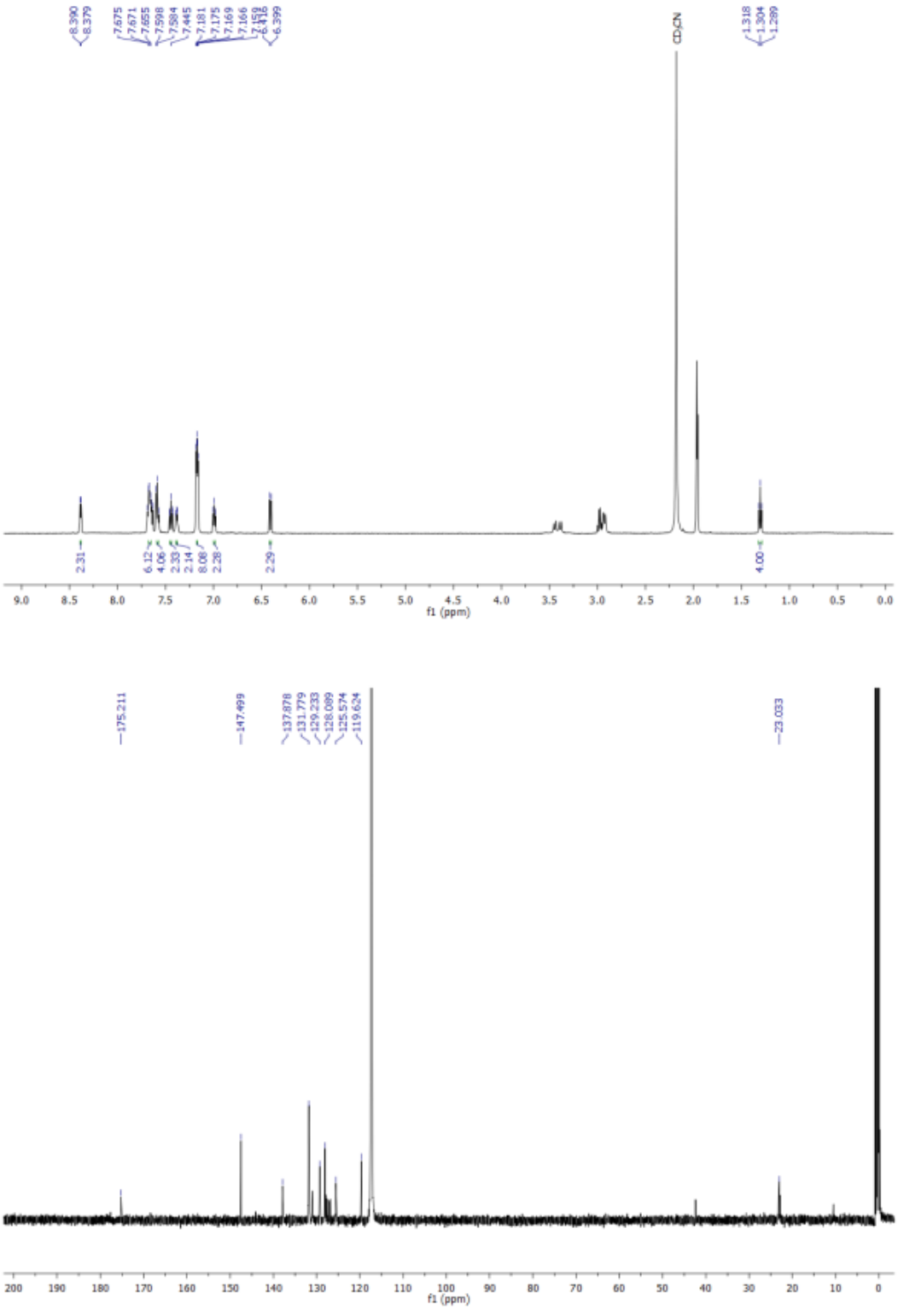

Figure S5. ^{1}H NMR (500 MHz, CD_3CN) and $^{13}C\{H\}$ NMR (125 MHz, CD_3CN) spectra of **7**.

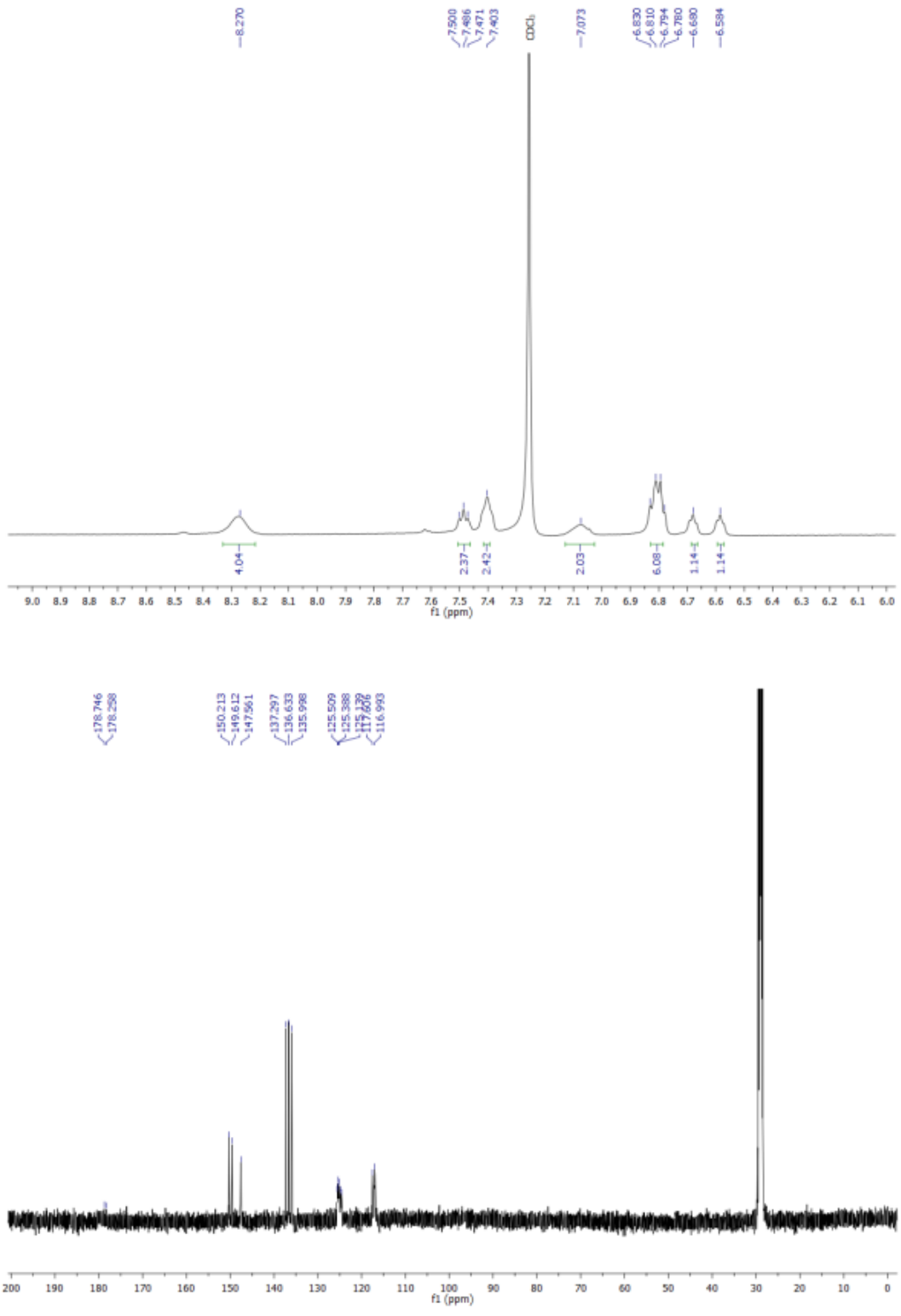

Figure S6. ^{1}H NMR (500 MHz, $CDCl_3$) and $^{13}C\{H\}$ NMR (125 MHz, $CDCl_3$) spectra of **8**.

S2.3 Catalytic reactions

Table S5. Reduction of **1a** to **1b** catalyzed by **1**-**8**, in the presence of CH_3NHNH_2, in 1 mL CH_3OH at 70°C and for 4 h.

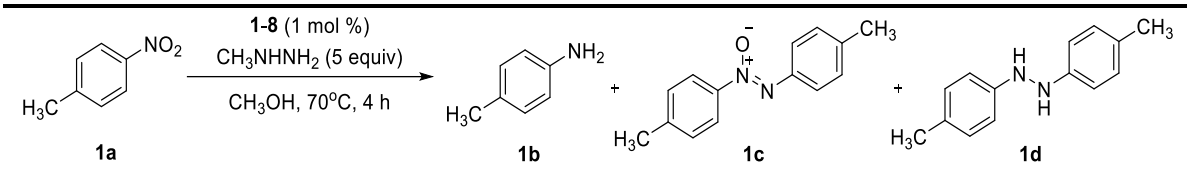

Catalyst[a]	Conversion (%)[b]	**1b** (%)[c]	**1c** (%)[c]	**1d** (%)[c]
1	65	65	-	-
2	95	95	-	-
3	55	55	-	-
4	40	40	-	-
5	85	85	-	-
6	70	70	-	-
7	40	40	-	-
8	55	55	-	-
$[Co(acac)_3]$	30%	30%	-	-
No catalyst	<10%	<10%	-	-

[a] **1a** (0.2 mmol), CH_3NHNH_2 (5 equiv, 1 mmol), catalysts (1 mol %), in CH_3OH, at 70°C and for 4 h. [b] Conversion percentages (%) of substrate **1a** were measured by ^1H NMR spectroscopy after addition of a specific amount of 1,3-dimethoxybenzene as internal standard. [c] Product yields were measured by ^1H NMR spectroscopy based on the integration of the appropriate proton peaks.

S2.3.1 ^{1}H NMR spectra of catalytic reaction product **1b** in the presence of complexes **1**-**8**

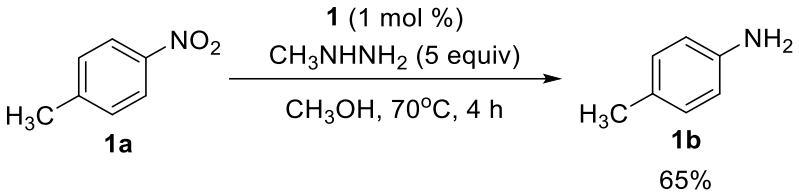

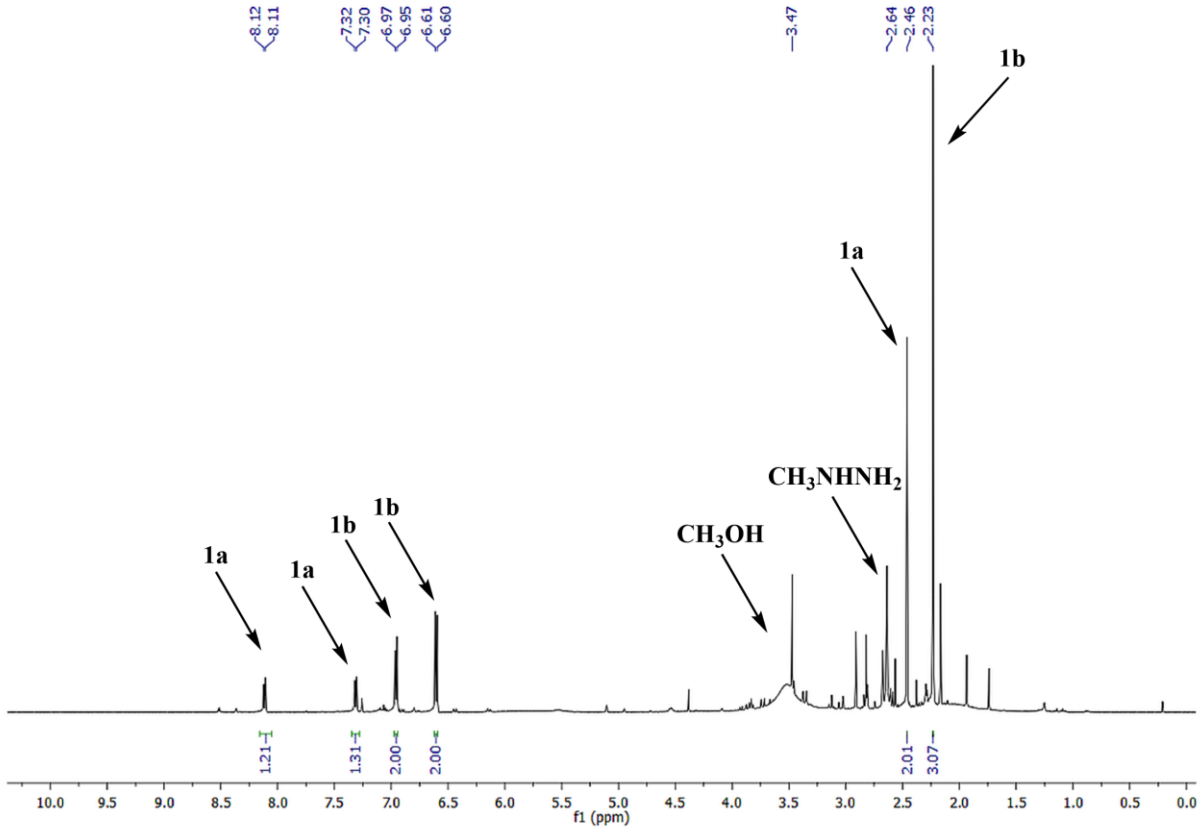

Figure S7. ^{1}H NMR spectrum of crude reaction mixture of the reduction of **1a** in the presence **1** and CH_3NHNH_2.

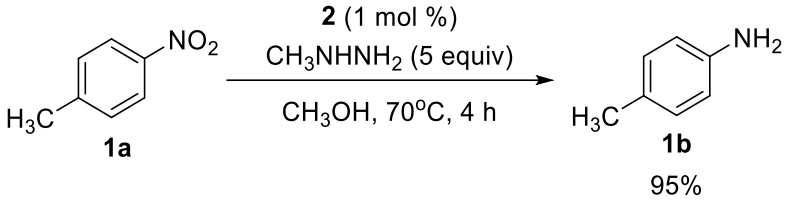

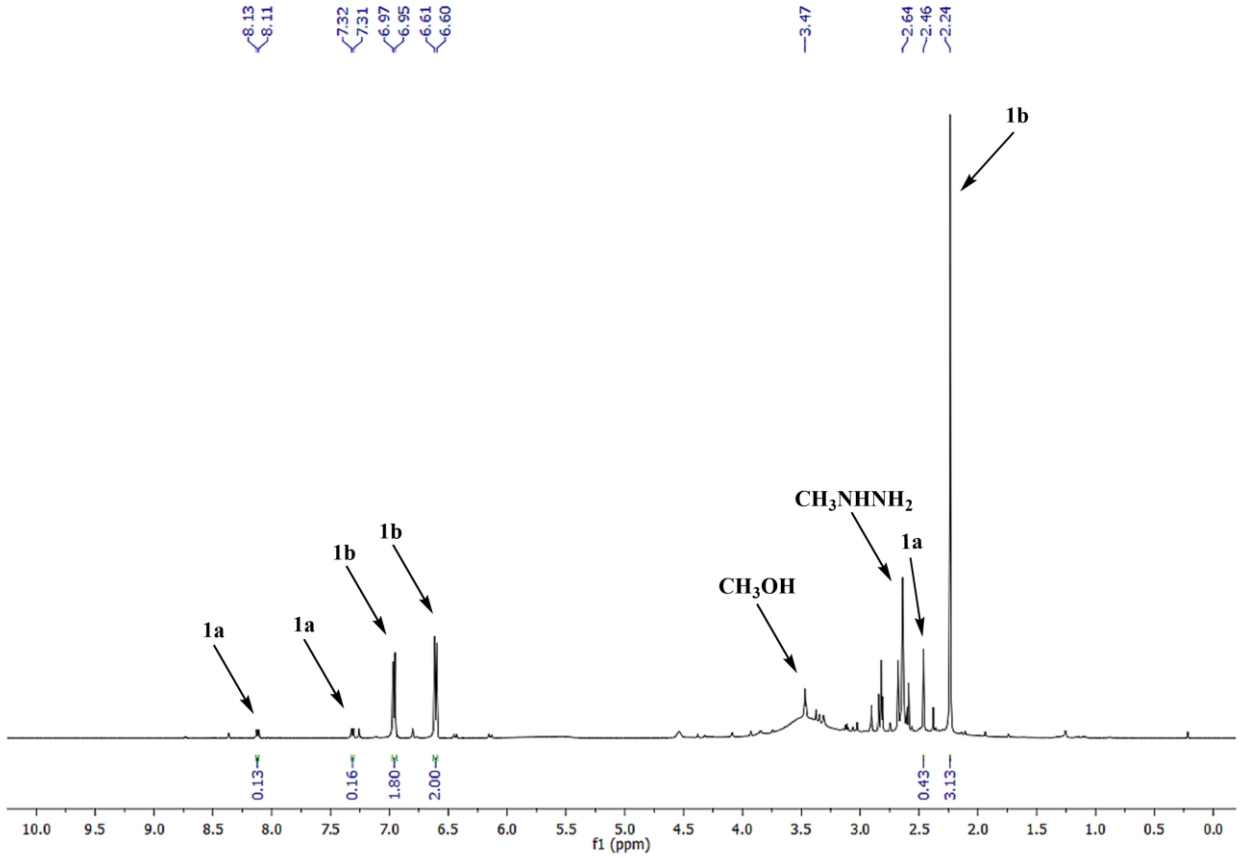

Figure S8. ^{1}H NMR spectrum of crude reaction mixture of the reduction of **1a** in the presence of **2** and CH_3NHNH_2.

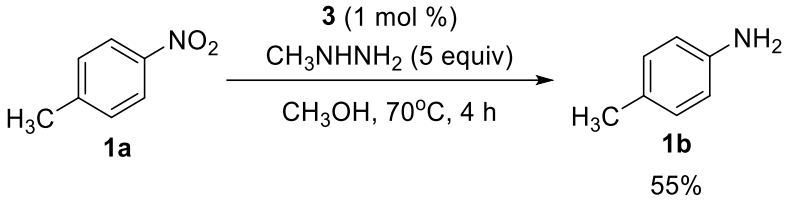

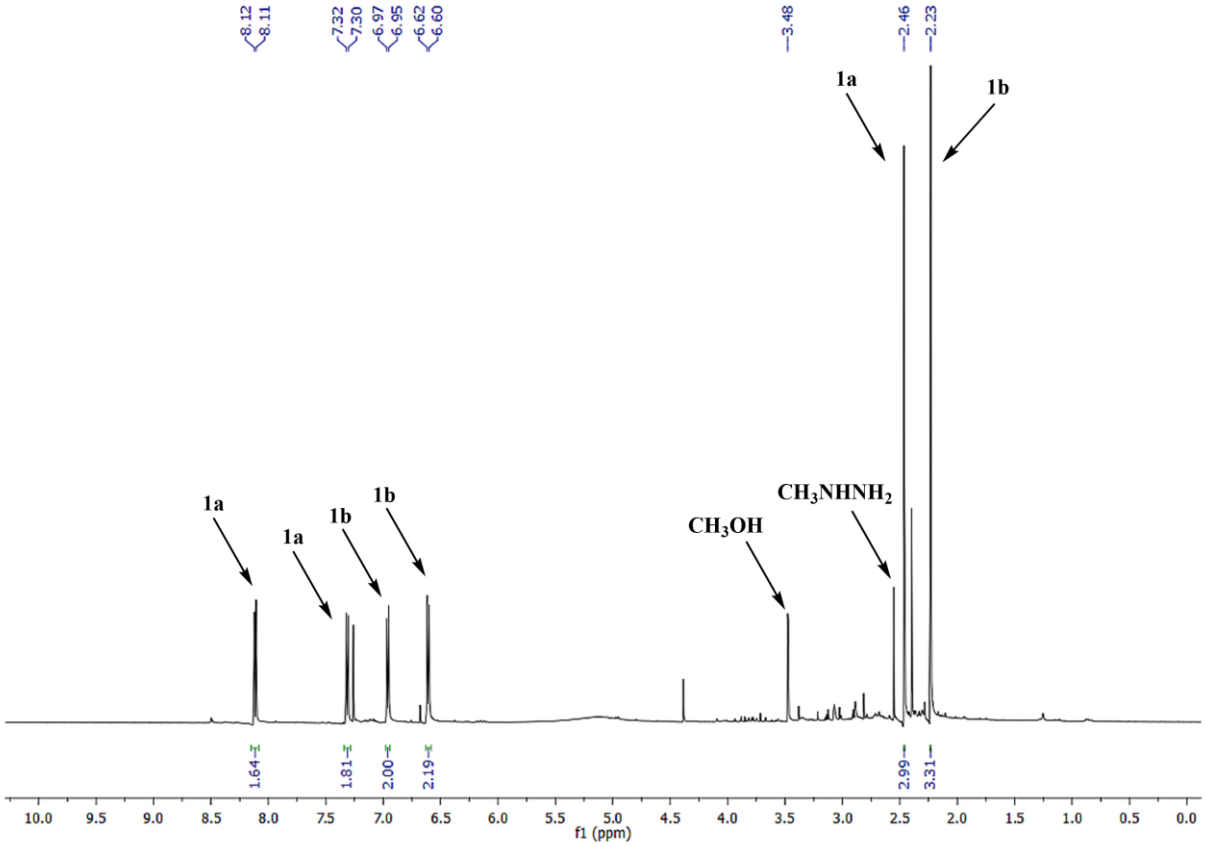

Figure S9. ^{1}H NMR spectrum of crude reaction mixture of the reduction of **1a** in the presence of **3** and CH_3NHNH_2.

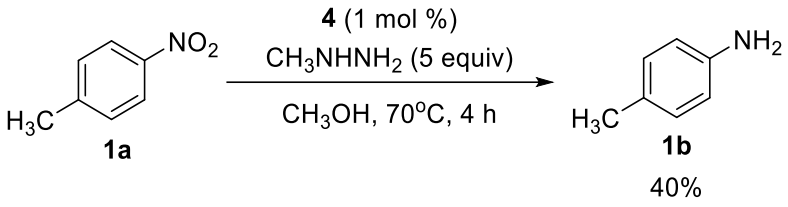

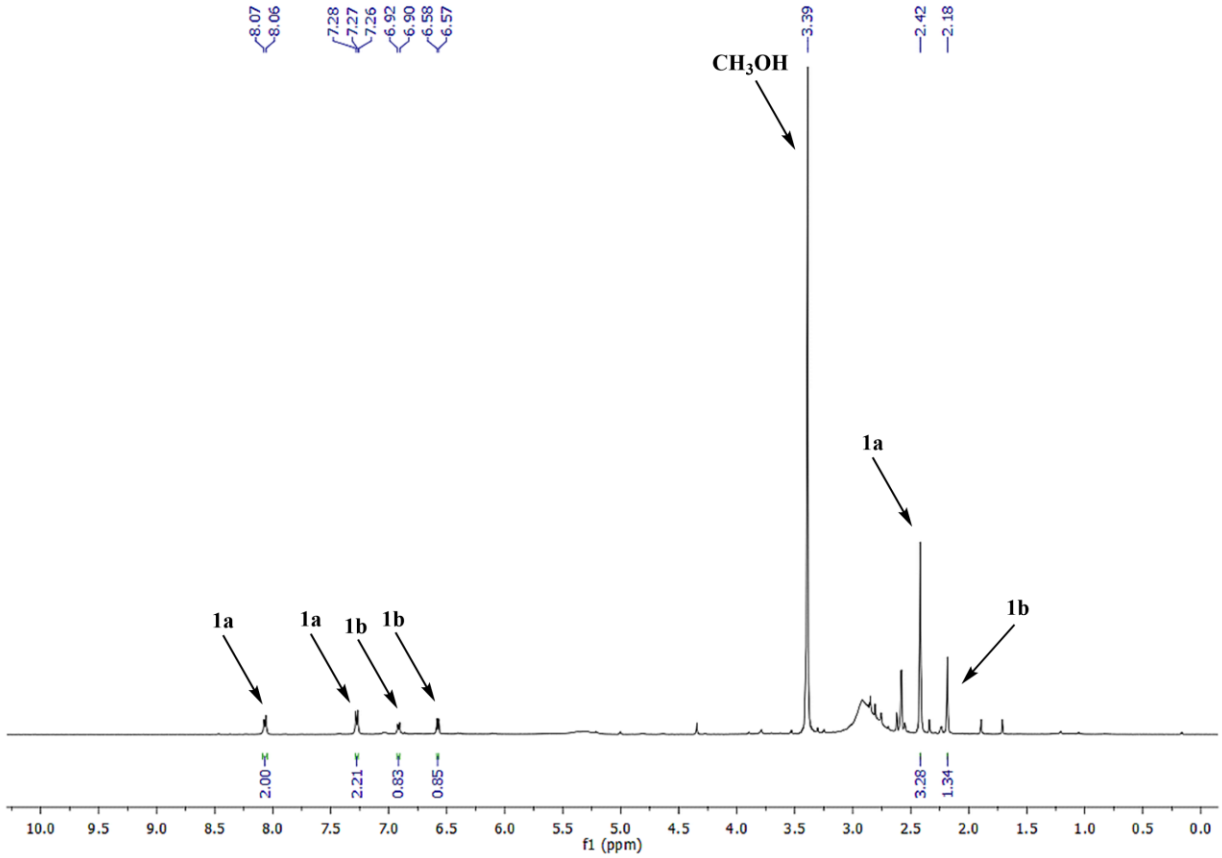

Figure S10. ^{1}H-NMR spectrum of crude reaction mixture of the reduction of **1a** in the presence of **4** and CH_3NHNH_2.

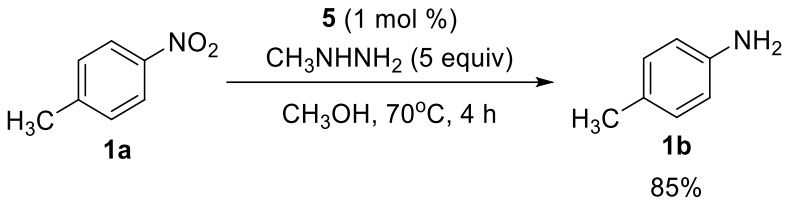

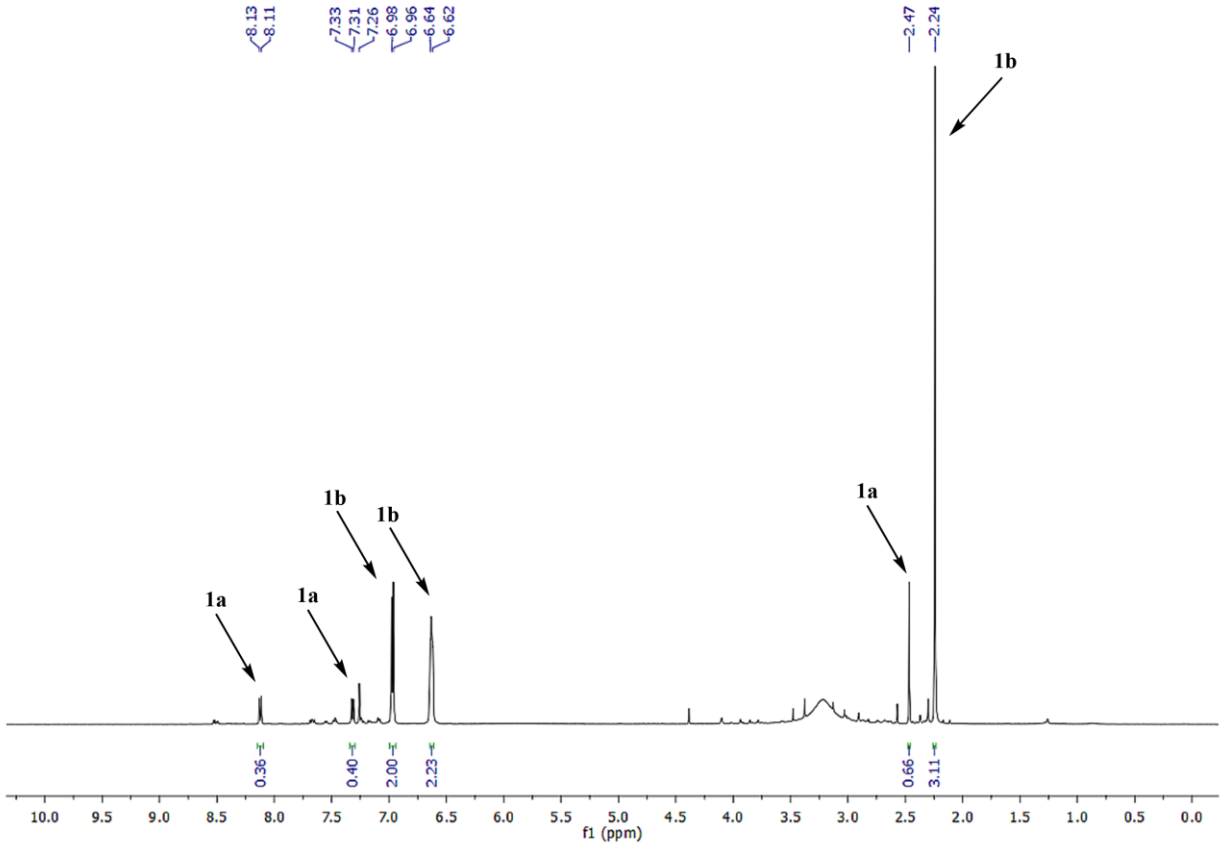

Figure S11. ^{1}H NMR spectrum of crude reaction mixture of the reduction of **1a** in the presence of **5** and CH_3NHNH_2.

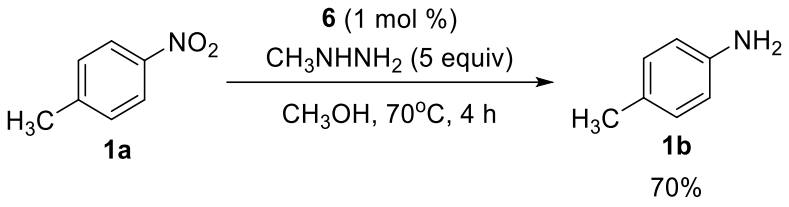

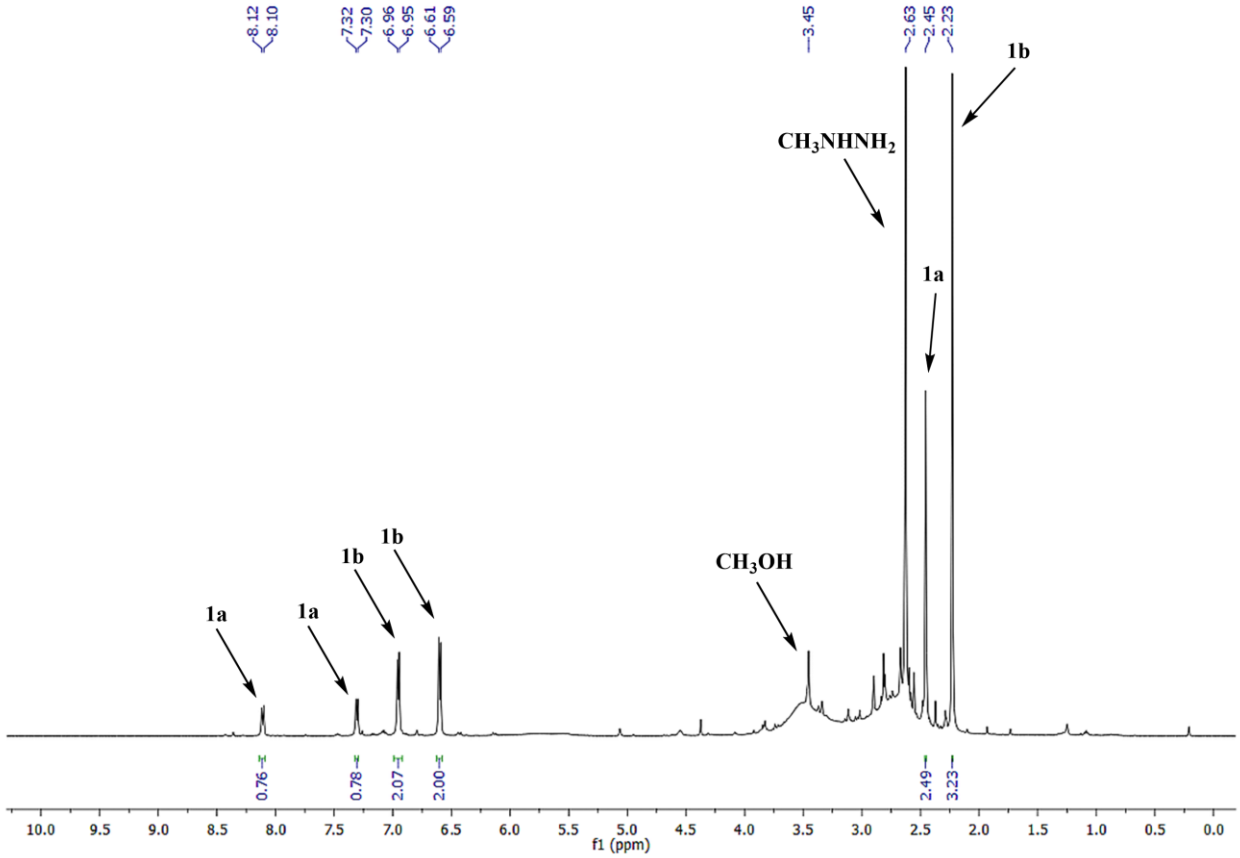

Figure S12. ^{1}H NMR spectrum of crude reaction mixture of the reduction of **1a** in the presence of **6** and CH_3NHNH_2.

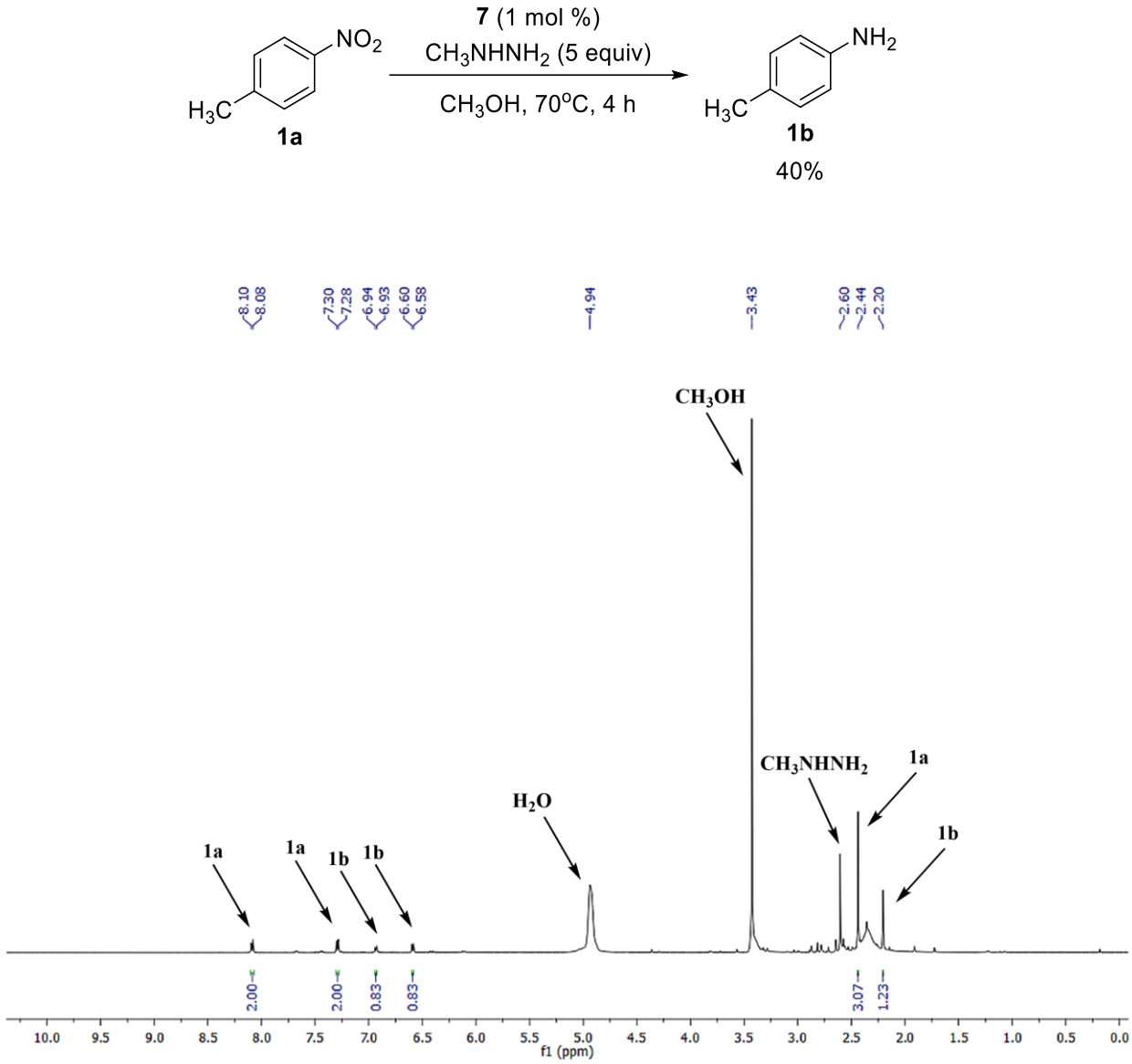

Figure S13. ^{1}H-NMR spectrum of crude reaction mixture of the reduction of **1a** in the presence of **7** and CH_3NHNH_2.

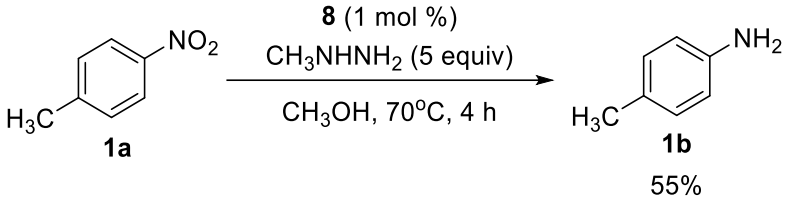

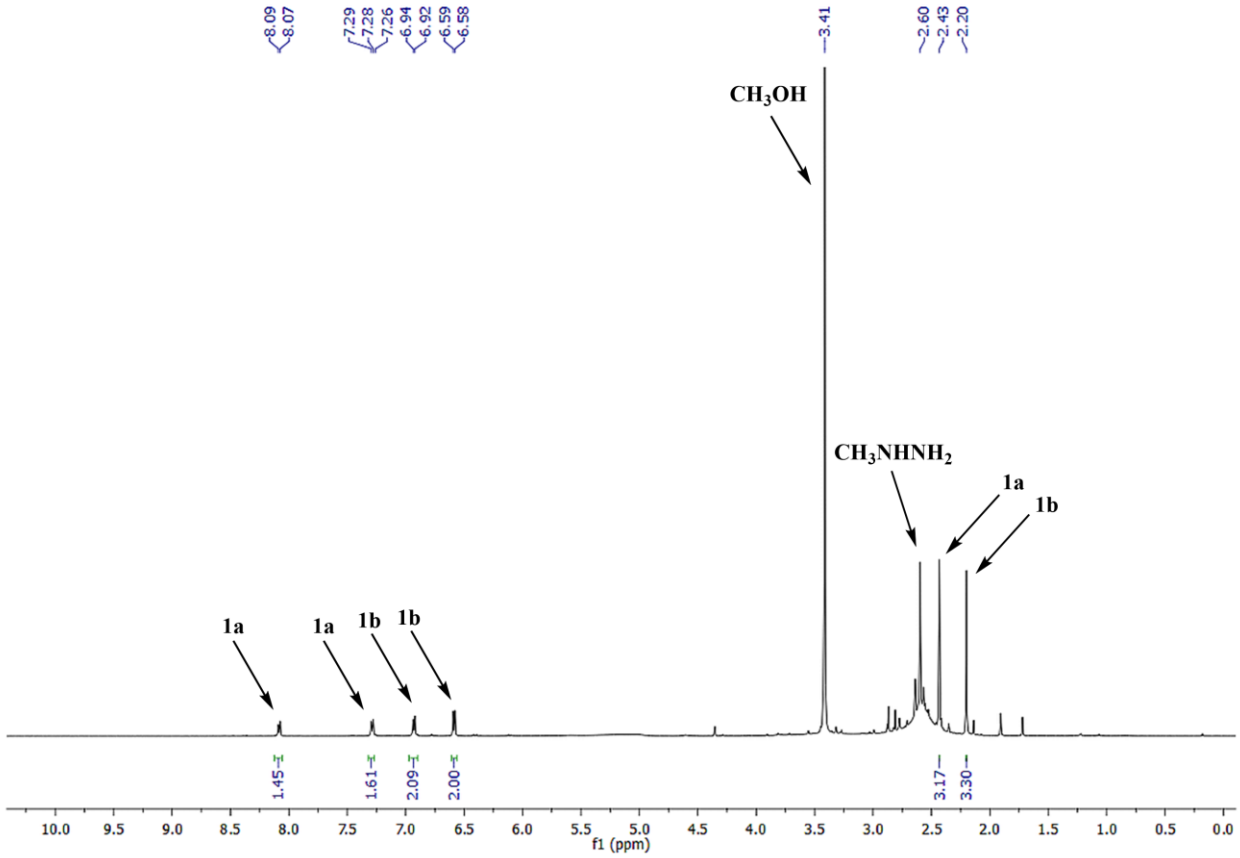

Figure S14. ^{1}H NMR spectrum of crude reaction mixture of the reduction of **1a** in the presence of **8** and CH_3NHNH_2.

S2.3.2 ^{1}H and $^{13}C\{H\}$ NMR spectra of catalytic reaction products **1b**-**14b**, **16b** and **17c** in the presence of complex **2**

p-Toluidine (**1b**):[4] brown solid, (19 mg, yield: 86%). ^{1}H NMR (500 MHz, $CDCl_3$): δ (ppm) 6.97 (d, J = 7.6 Hz, 2 H), 6.62 (d, J = 7.6 Hz, 2 H), 3.56 (br s, 2 H), 2.25 (s, 3 H). $^{13}C\{H\}$ NMR (125 MHz, $CDCl_3$): δ (ppm) 143.8, 129.8, 127.8, 115.3, 20.5.

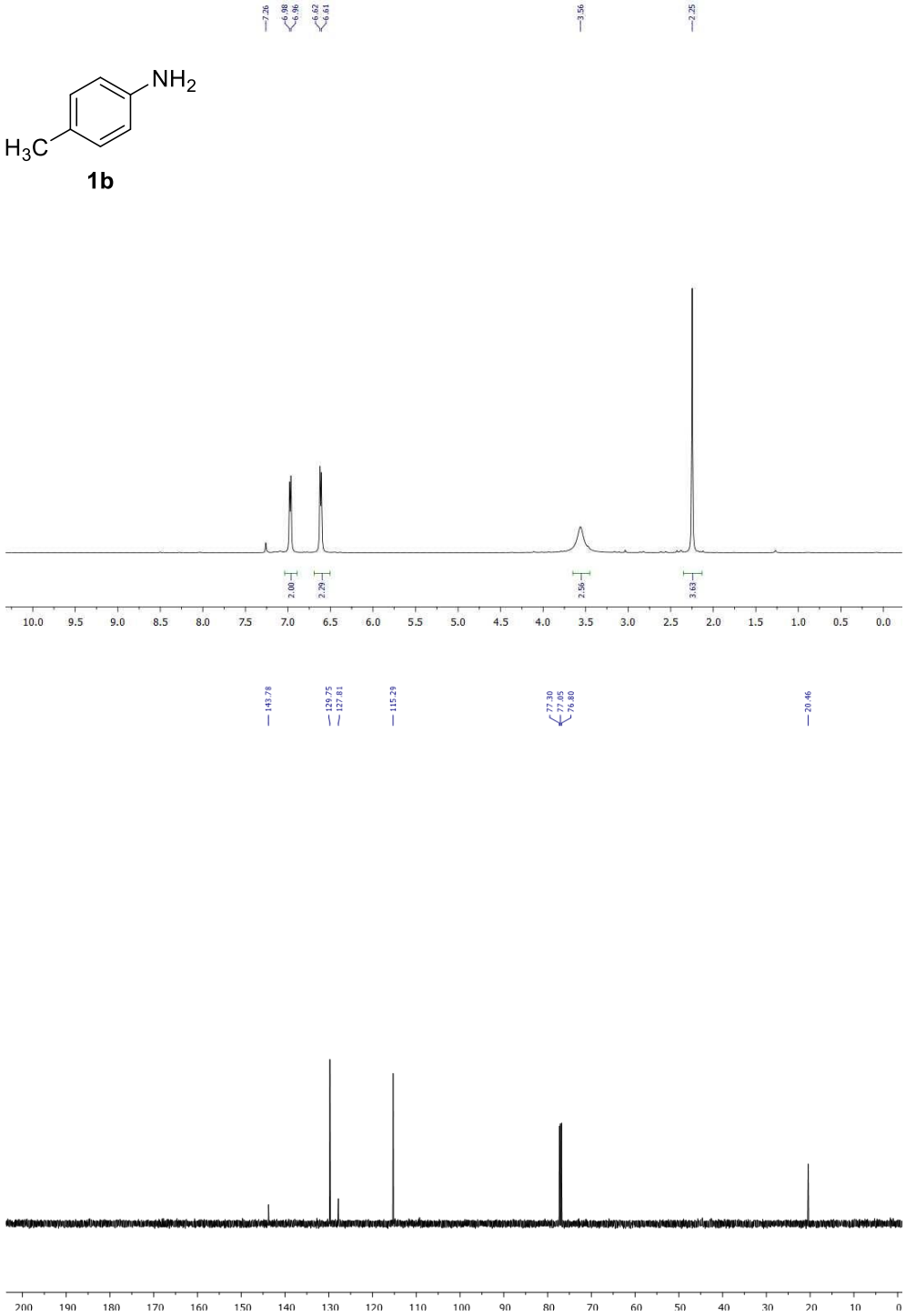

Figure S15. ^{1}H NMR (500 MHz, $CDCl_3$) and $^{13}C\{H\}$ NMR (125 MHz, $CDCl_3$) spectra of **1b**.

m-Toluidine (**2b**):[4] light yellow liquid, (18 mg, yield: 82%). ^{1}H NMR (500 MHz, $CDCl_3$): δ (ppm) 7.10 (t, J = 7.6 Hz, 1 H), 6.65 (d, J = 7.5 Hz, 1 H), 6.56-6.54 (m, 2 H), 3.54 (br s, 2 H), 2.32 (s, 3 H). ^{13}C{H} NMR (125 MHz, $CDCl_3$): δ (ppm) 146.2, 139.0, 129.1, 119.4, 115.9, 112.2, 21.4.

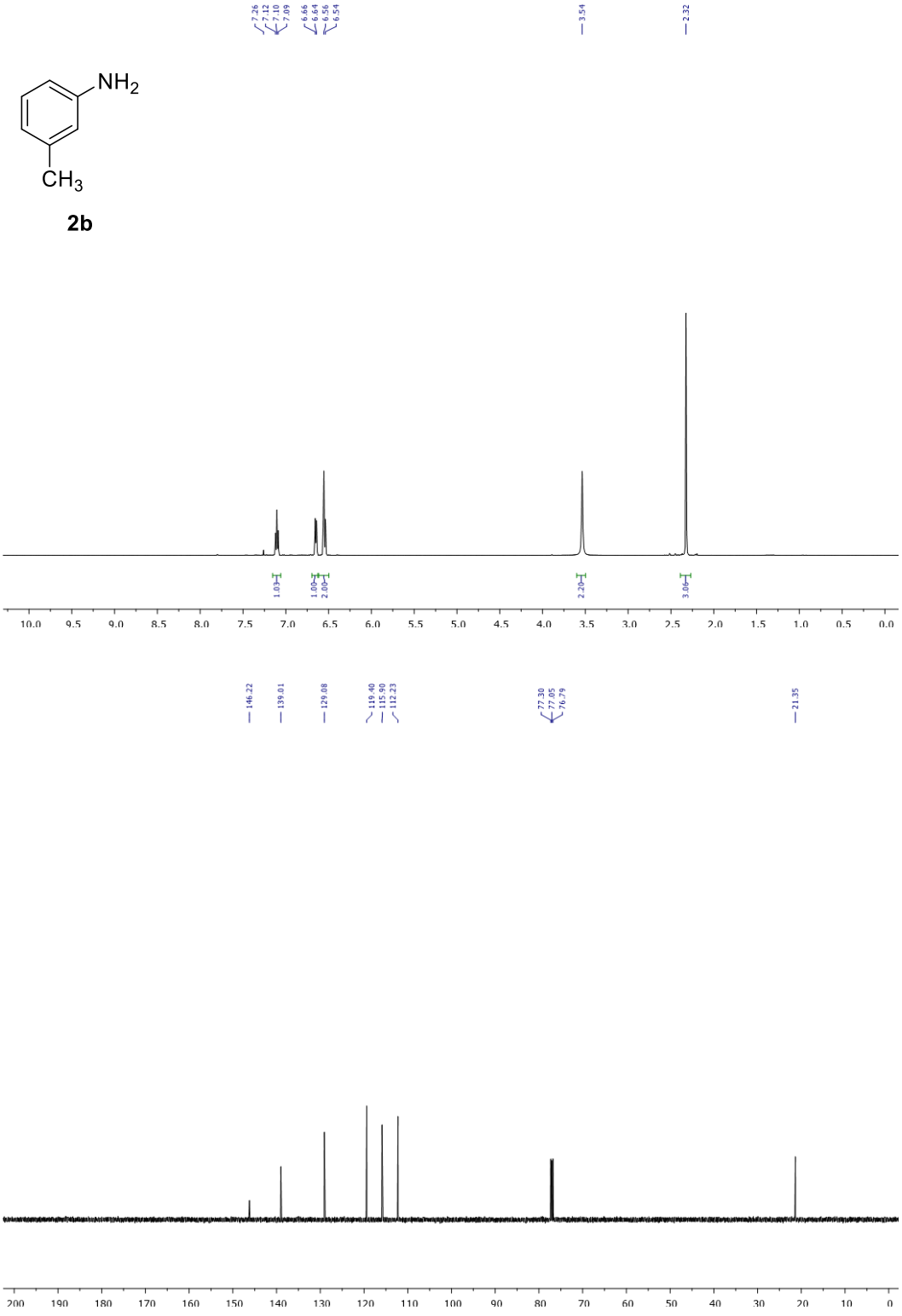

Figure S16. ^{1}H NMR (500 MHz, $CDCl_3$) and ^{13}C{H} NMR (125 MHz, $CDCl_3$) spectra of **2b**.

2,3-dimethylaniline (**3b**): [4] light brown solid, (20 mg, yield 83%). ^{1}H NMR (500 MHz, $CDCl_3$): δ (ppm) 6.94 (t, J = 7.7 Hz, 1 H), 6.68 (d, J = 7.4 Hz, 1 H), 6.65 (d, J = 7.9 Hz, 1 H), 2.27 (s, 3 H), 2.11 (s, 3 H). ^{13}C{H} NMR (125 MHz, $CDCl_3$): δ (ppm) 144.5, 137.2, 126.0, 120.9, 120.7, 113.2, 20.5, 12.7.

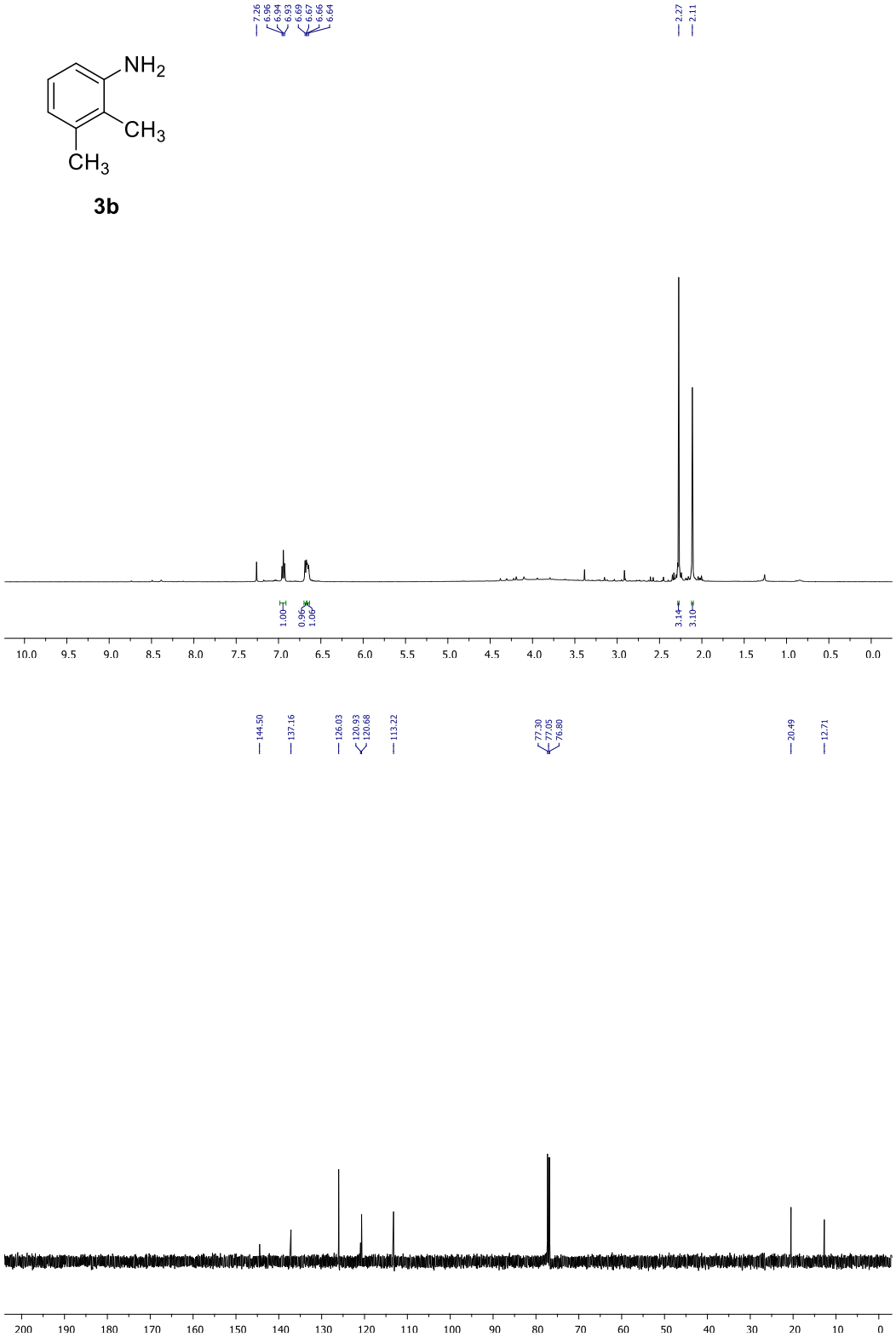

Figure S17. ^{1}H NMR (500 MHz, $CDCl_3$) and ^{13}C{H} NMR (125 MHz, $CDCl_3$) spectra of **3b**.

benzene-1,4-diamine (**4b**):[7] brown solid, (17 mg, yield 78%). ^{1}H NMR (500 MHz, $CDCl_3$): δ (ppm) 6.56 (s, 4 H). ^{13}C{H} NMR (125 MHz, $CDCl_3$): δ (ppm) 138.5, 116.8.

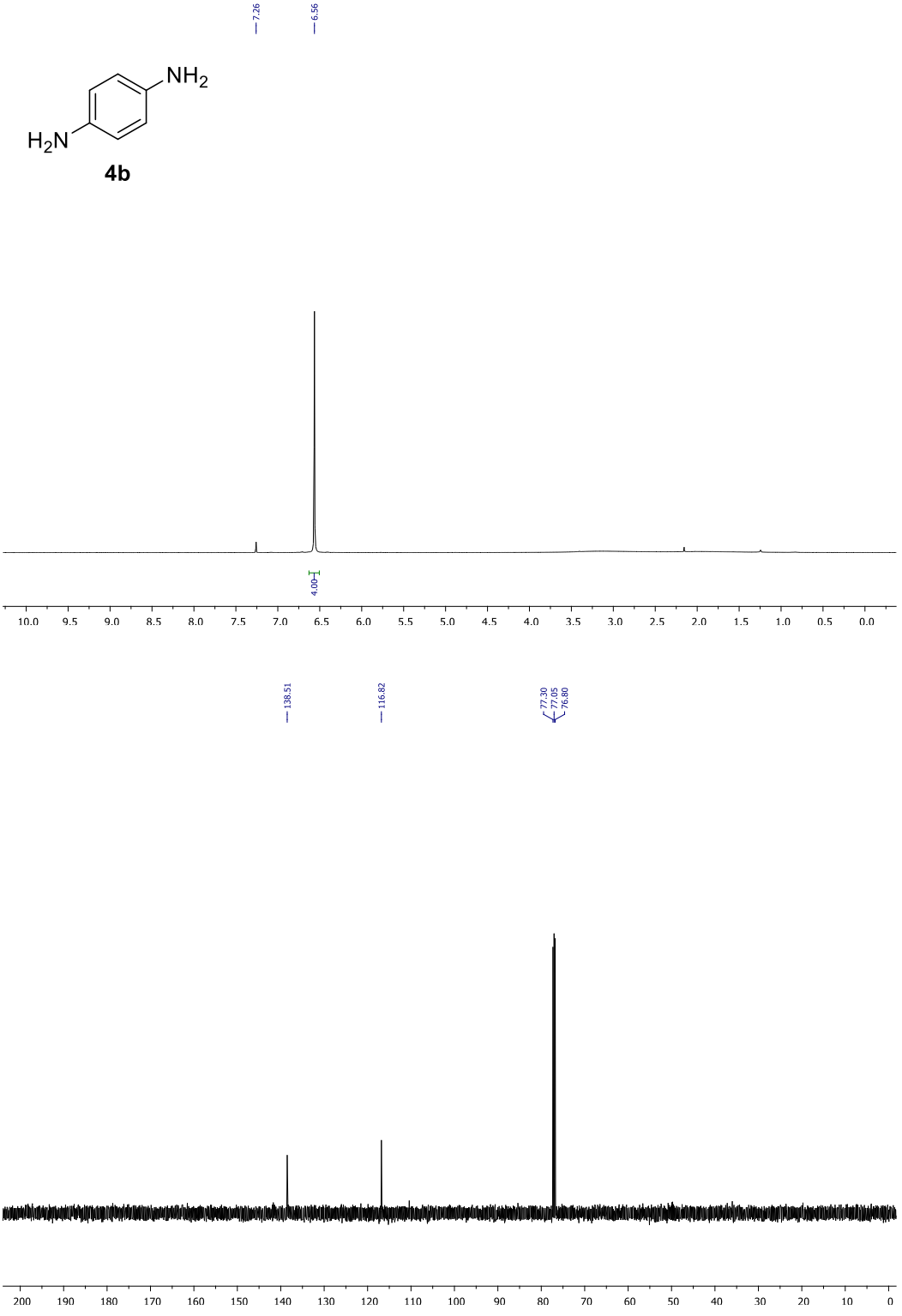

Figure S18. ^{1}H NMR (500 MHz, $CDCl_3$) and ^{13}C{H} NMR (125 MHz, $CDCl_3$) spectra of **4b**.

m-Anisidine (**5b**):[5] light yellow liquid, (20 mg, yield: 81%). ^{1}H NMR (500 MHz, $CDCl_3$): δ (ppm) 7.06 (t, J = 7.9 Hz, 1 H), 6.34-6.30 (dd, J = 7.9, 1.8 Hz, 2 H), 6.25 (s, 1 H), 3.76 (s, 3 H). ^{13}C{H} NMR (125 MHz, $CDCl_3$): 160.7, 147.7, 130.1, 107.9, 103.9, 101.1, 55.1.

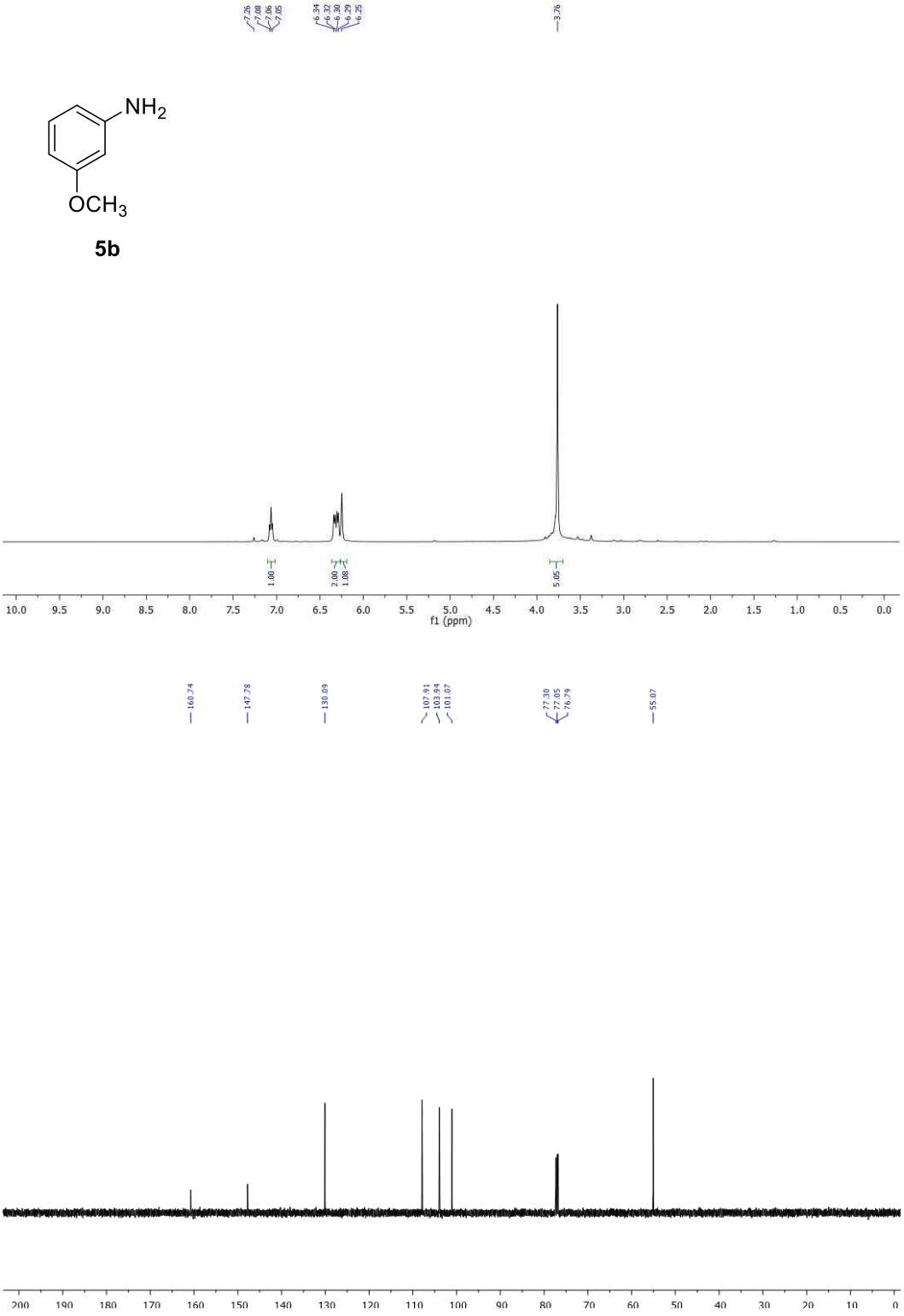

Figure S19. ^{1}H NMR (500 MHz, $CDCl_3$) and ^{13}C{H} NMR (125 MHz, $CDCl_3$) spectra of **5b**.

p-Chloroaniline (**6b**):[5] light yellow solid, (21 mg, yield: 81%). ^{1}H NMR (500 MHz, $CDCl_3$): δ (ppm) 7.09 (d, J = 8.1 Hz, 2 H), 6.60 (d, J = 8.1 Hz, 2 H), 3.67 (br s, 2 H). ^{13}C{H} NMR (125 MHz, $CDCl_3$): δ (ppm) 144.9, 129.1, 123.2, 116.2.

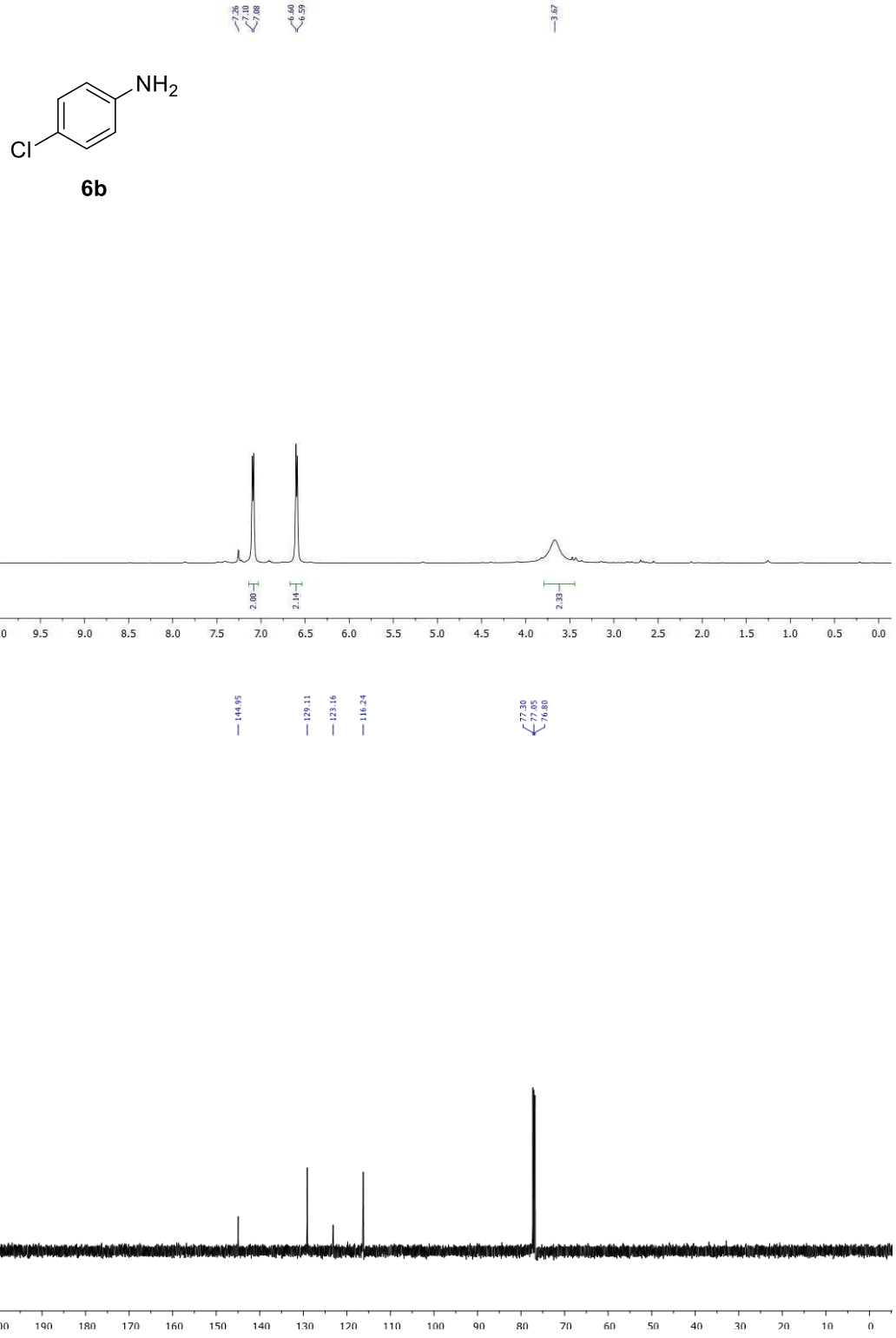

6b

Figure S20. ^{1}H NMR (500 MHz, $CDCl_3$) and ^{13}C{H} NMR (125 MHz, $CDCl_3$) spectra of **6b**.

p-Bromoaniline (**7b**):[5] brown liquid, (27 mg, yield: 79%). ^{1}H NMR (500 MHz, $CDCl_3$): δ (ppm) 7.23 (d, J = 7.9 Hz, 2 H), 6.56 (d, J = 7.9 Hz, 2 H), ^{13}C{H} NMR (125 MHz, $CDCl_3$): 145.4, 132.0, 116.7, 110.2.

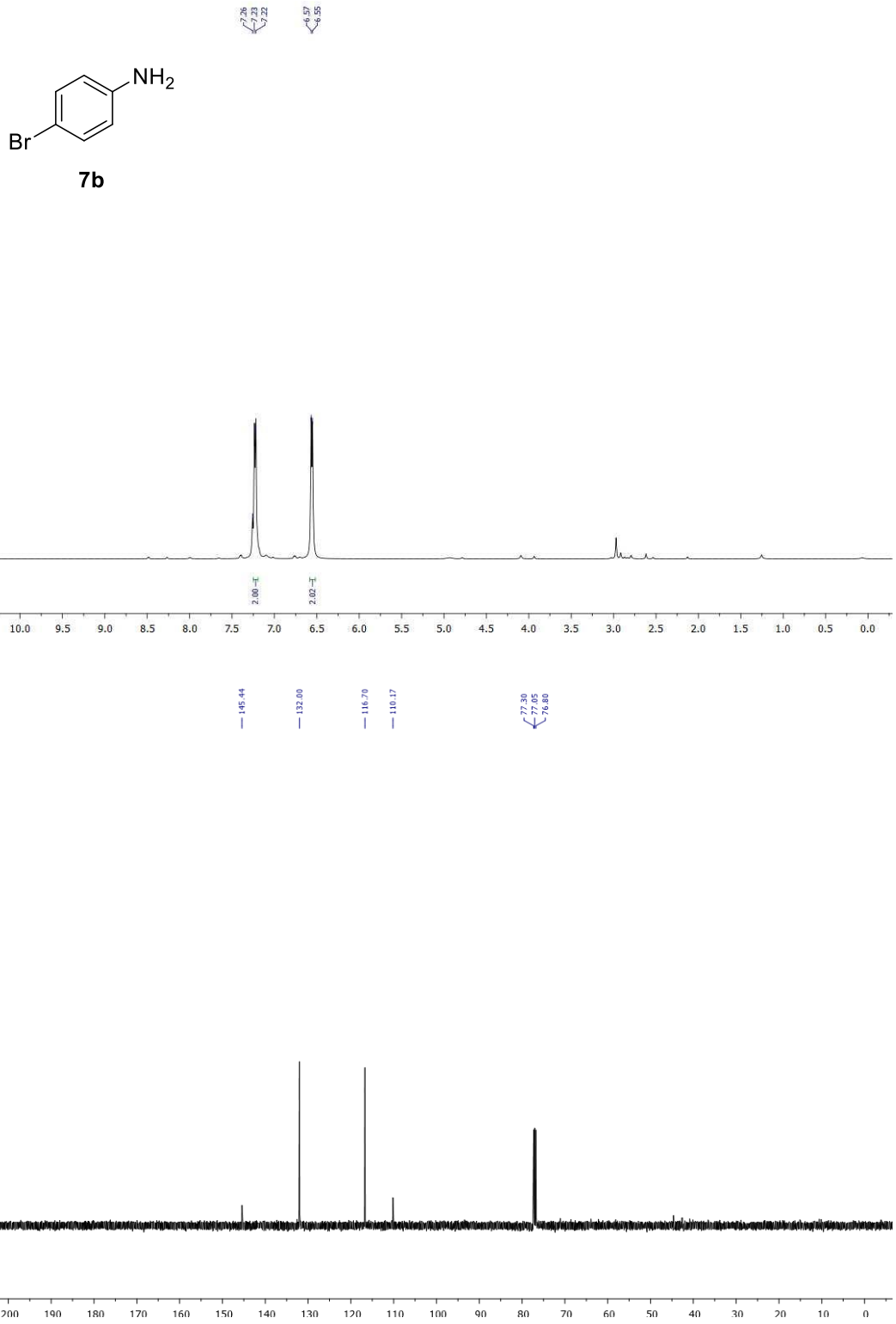

Figure S21. ^{1}H NMR (500 MHz, $CDCl_3$) and ^{13}C{H} NMR (125 MHz, $CDCl_3$) spectra of **7b**.

Methyl 4-aminobenzoate (**8b**):[5] light yellow solid, (23 mg, yield: 77%). ^{1}H NMR (500 MHz, $CDCl_3$): δ (ppm) 7.85 (d, J = 8.5 Hz, 2 H), 6.63 (d, J = 8.5 Hz, 2 H), 4.05 (br s, 2 H), 3.85 (s, 3 H). ^{13}C{H} NMR (125 MHz, $CDCl_3$): δ (ppm) 167.2, 150.9 , 131.6, 119.6, 113.8, 51.6.

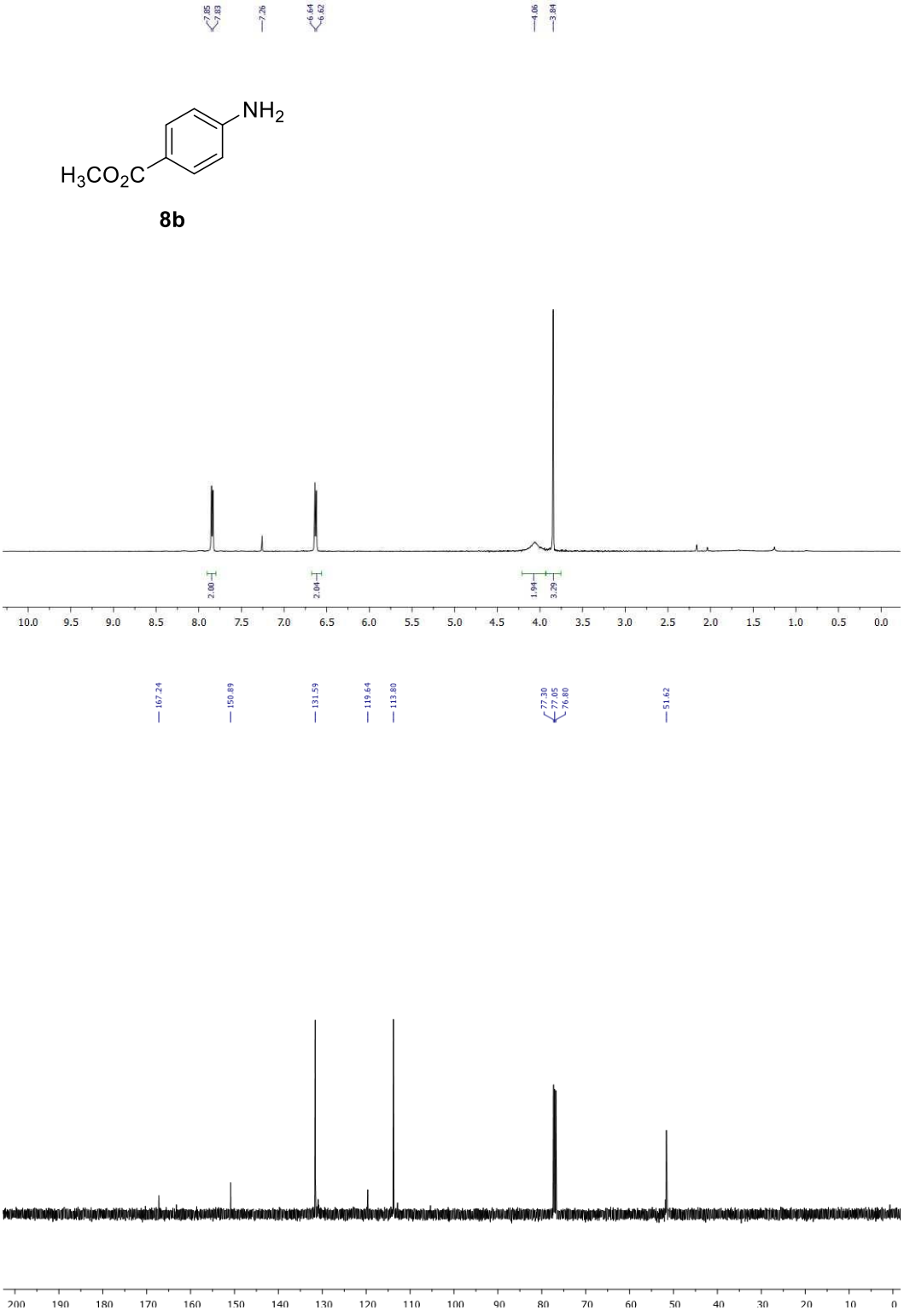

Figure S22. ^{1}H NMR (500 MHz, $CDCl_3$) and ^{13}C{H} NMR (125 MHz, $CDCl_3$) spectra of **8b**.

1-(4-aminophenyl)ethan-1-one (**9b**):[5] yellow solid, (21 mg, yield: 75%). ^{1}H NMR (500 MHz, $CDCl_3$): δ (ppm) 7.80 (d, J = 8.2 Hz, 2 H), 6.66 (d, J = 8.0 Hz, 2 H), 2.50 (s, 3 H). ^{13}C{H} NMR (125 MHz, $CDCl_3$): δ (ppm) 196.5, 150.8, 130.8, 113.9, 26.1.

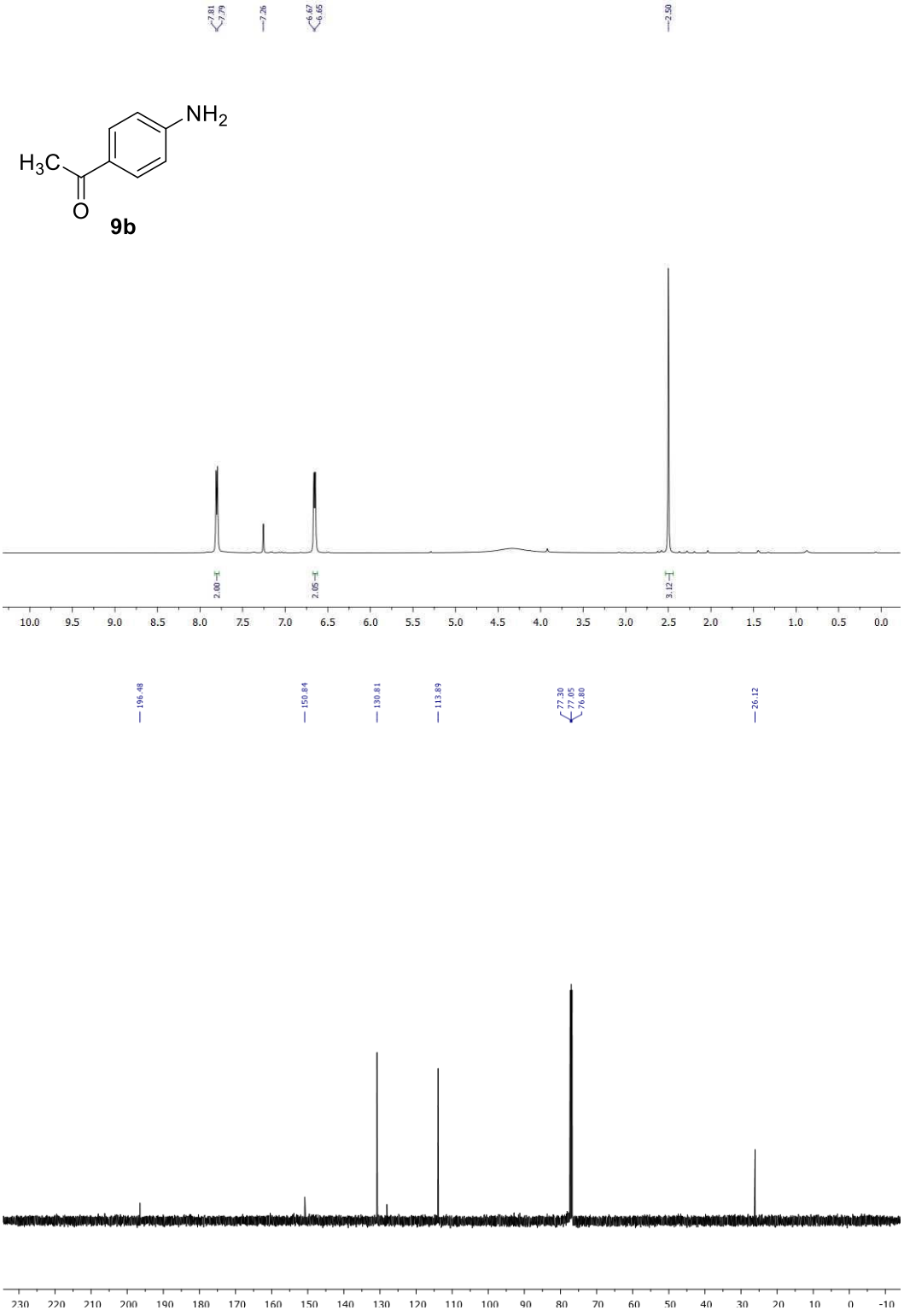

Figure S23. ^{1}H NMR (500 MHz, $CDCl_3$) and ^{13}C{H} NMR (125 MHz, $CDCl_3$) spectra of **9b**.

m-aminobenzonitrile (**10b**):[5] brown solid, (18 mg, yield: 75%). ^{1}H NMR (500 MHz, $CDCl_3$): δ (ppm) 7.21 (t, J = 7.8 Hz, 1 H), 7.00 (d, J = 7.8 Hz, 1 H), 6.89 (s, 1 H), 6.86 (d, J = 8.9 Hz, 1 H), 3.92 (br s, 2 H). ^{13}C{H} NMR (125 MHz, $CDCl_3$): δ (ppm) 146.9, 130.0, 121.9, 119.2 (2C), 117.4, 112.9.

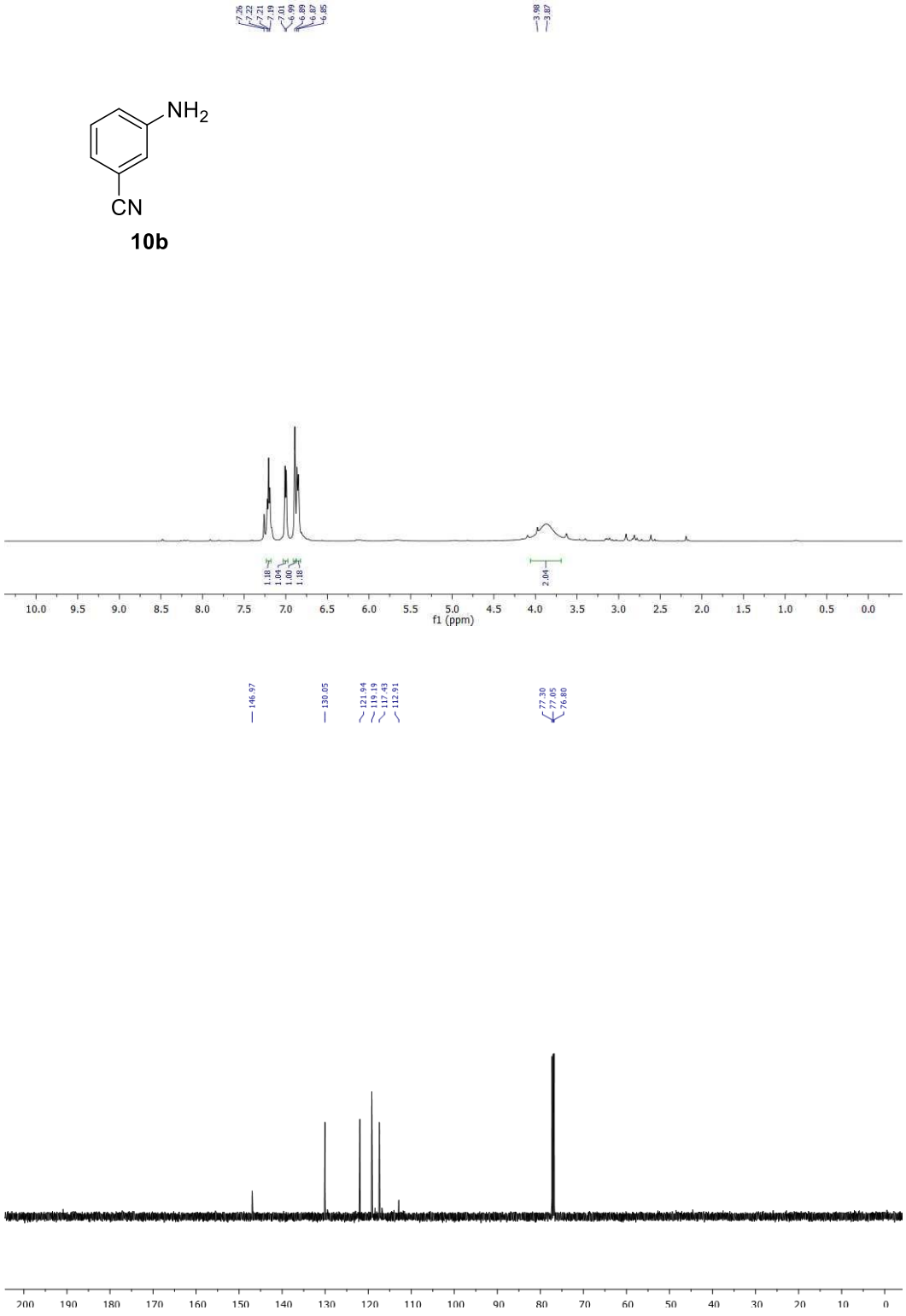

Figure S24. ^{1}H NMR (500 MHz, $CDCl_3$) and ^{13}C{H} NMR (125 MHz, $CDCl_3$) spectra of **10b**.

3-aminobenzenesulfonamide (**11b**):[5] yellow solid, (27 mg, yield: 78%). ^{1}H NMR (500 MHz, CD_3OD): *δ* (ppm) 7.24 (d, *J* = 7.8 Hz, 1 H), 7.22, (s, 1 H), 7.18 (d, *J* = 7.5 Hz, 1 H), 6.89 (d, *J* = 7.8 Hz, 1 H). ^{13}C{H} NMR (125 MHz, CD_3OD): 149.8, 145.2, 130.6, 119.3, 115.5, 112.7.

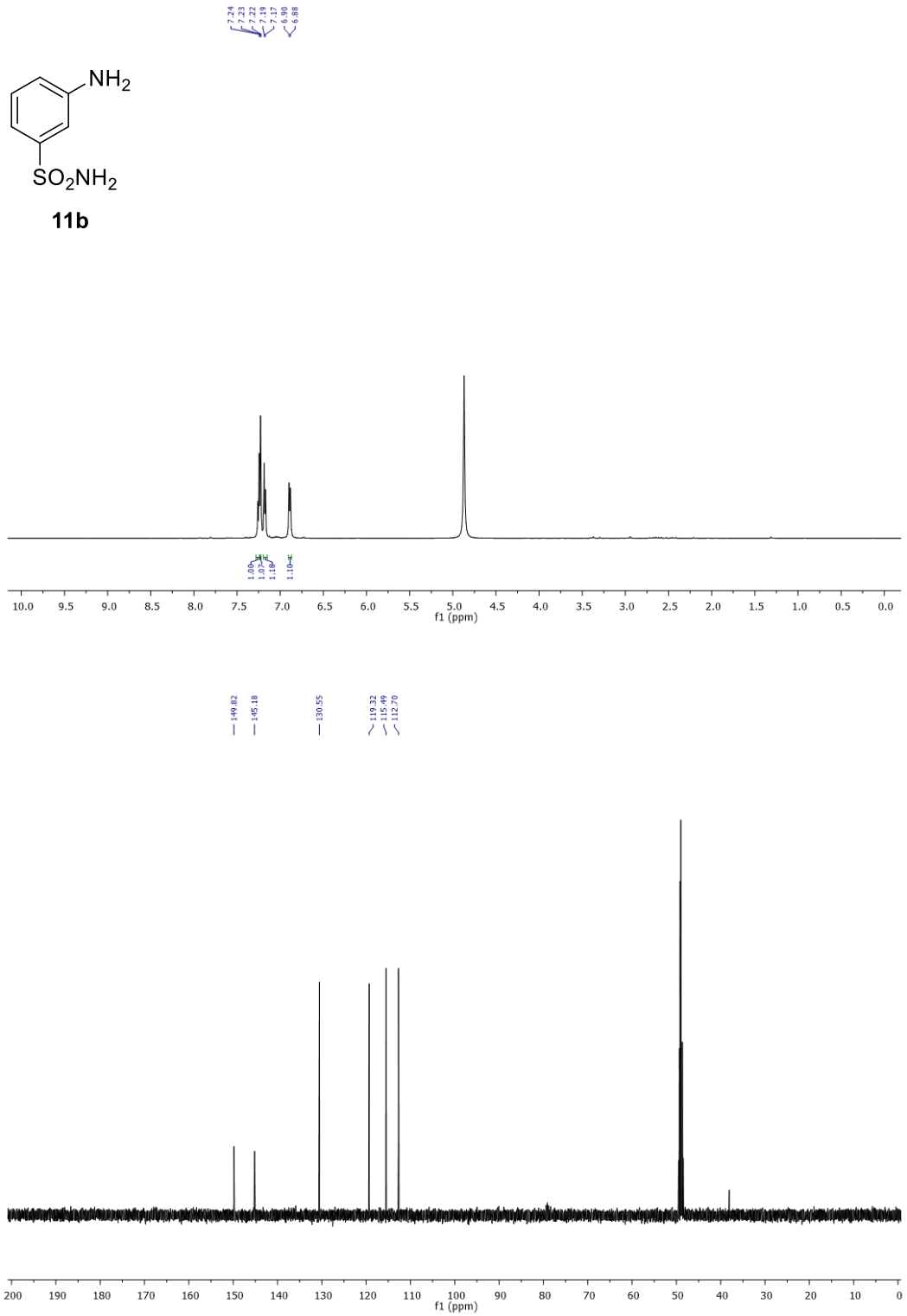

Figure S25. ^{1}H NMR (500 MHz, CD_3OD) and ^{13}C{H} NMR (125 MHz, CD_3OD) spectra of **11b**.

6-aminoisobenzofuran-1(3H)-one (**12b**):[5] yellow solid, (25 mg, yield: 83%). ^{1}H NMR (500 MHz, CD_3OD): δ (ppm) 7.29 (d, J = 7.8 Hz, 1 H), 7.08-7.05 (m, 2 H), 5.22 (s, 2 H). ^{13}C{H} NMR (125 MHz, CD_3OD): δ (ppm) 172.8, 149.3, 135.9, 125.9, 122.4, 121.8, 108.3, 69.9.

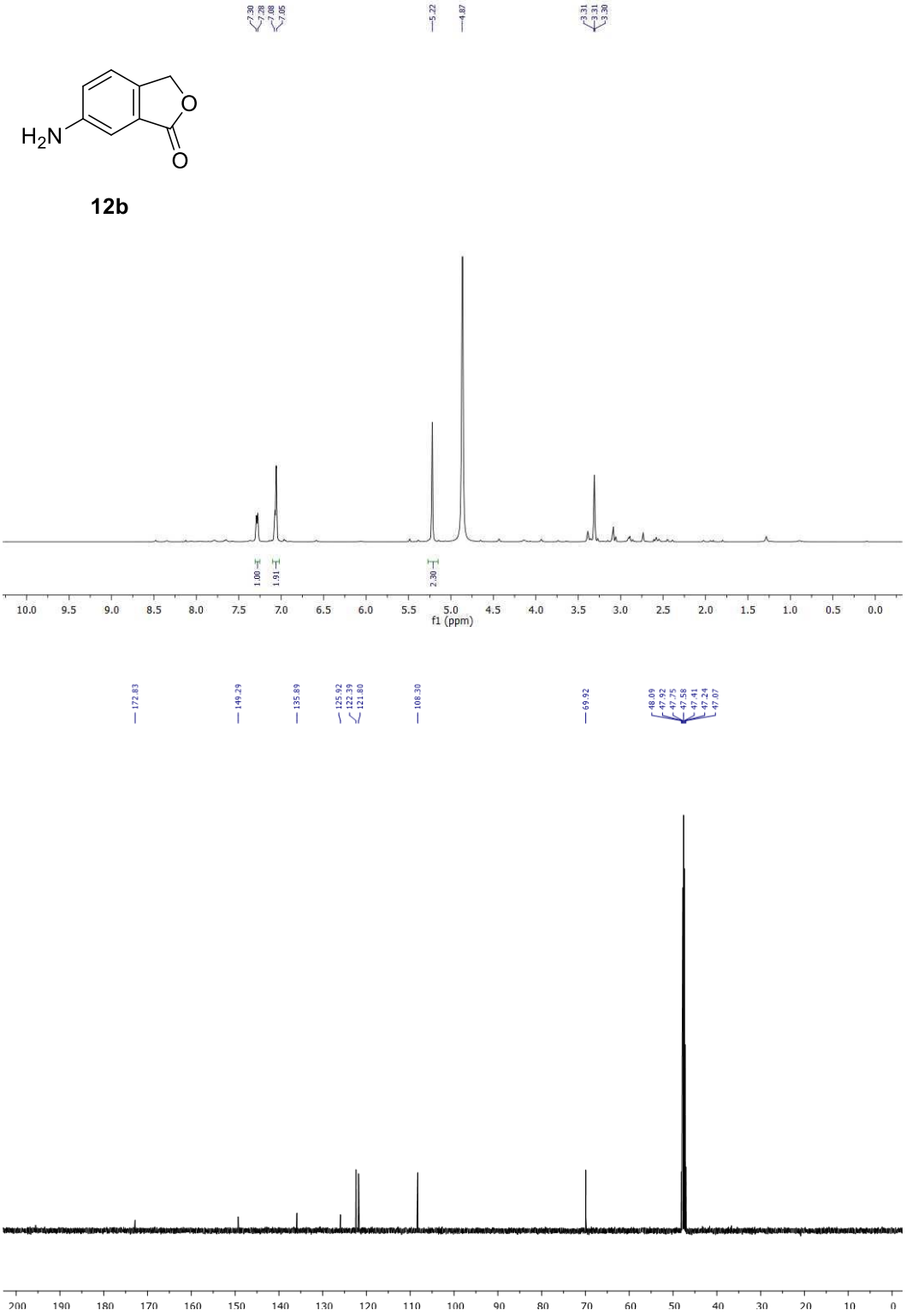

Figure S26. ^{1}H NMR (500 MHz, CD_3OD) and ^{13}C{H} NMR (125 MHz, CD_3OD) spectra of **12b**.

1H-benzo[d]imidazol-5-amine (**13b**):[5] brown solid, (22 mg, yield: 81%). ^{1}H NMR (500 MHz, CD_3OD): δ (ppm) 8.00 (s, 1 H), 7.37 (d, J = 9.0 Hz, 1 H), 6.93 (s, 1 H), 6.77 (d, J = 8.2 Hz, 1 H). ^{13}C{H} NMR (125 MHz, CD_3OD): δ (ppm) 144.9, 140.9, 139.7, 117.2, 114.8, 100.4.

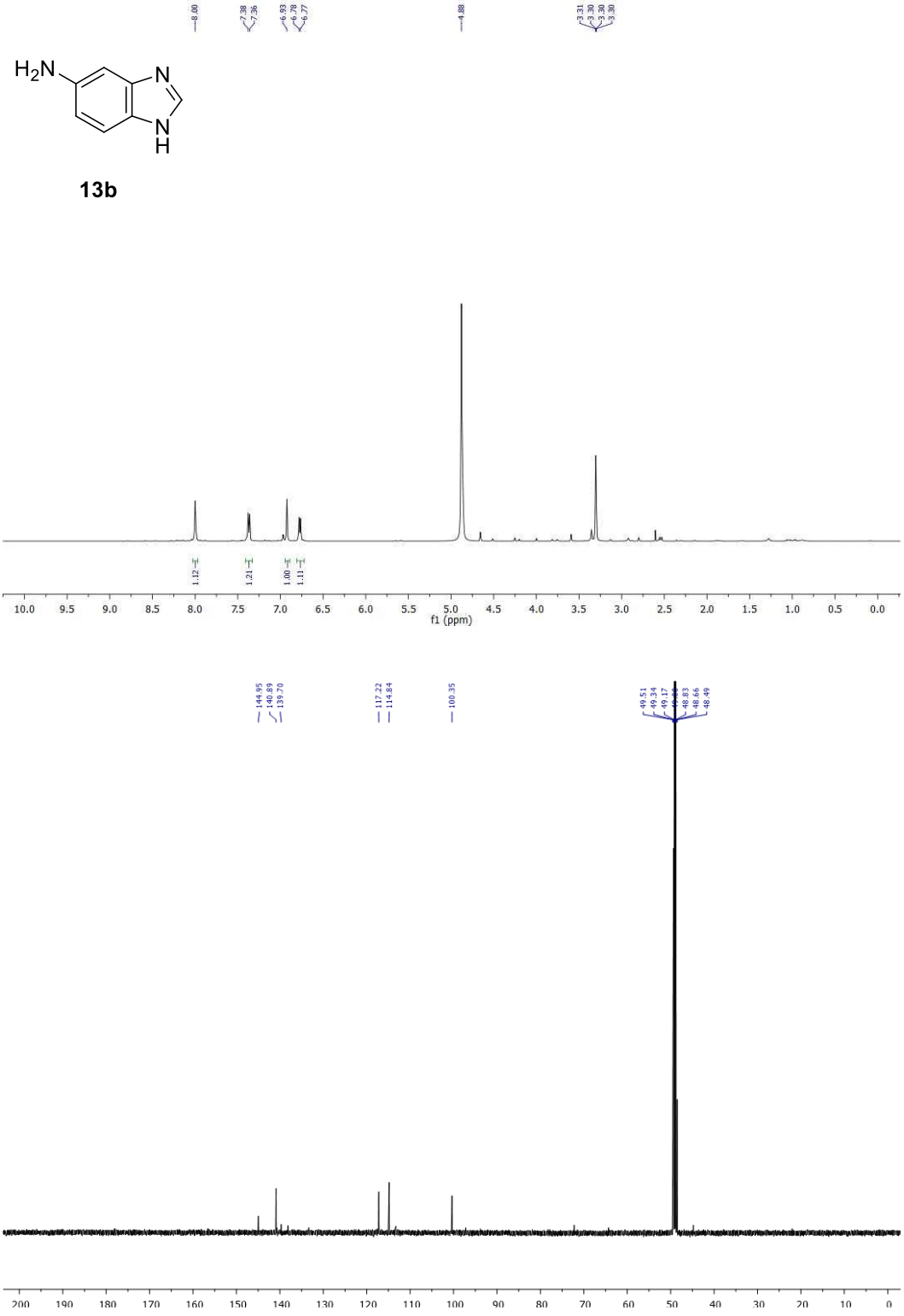

Figure S27. ^{1}H NMR (500 MHz, CD_3OD) and ^{13}C{H} NMR (125 MHz, CD_3OD) spectra of **13b**.

1H-indazol-5-amine (**14b**):[5] yellow liquid, (21 mg, yield: 79%). ^{1}H NMR (500 MHz, CD_3OD): δ (ppm) 7.79 (s, 1 H), 7.46 (d, J = 8.6 Hz, 1 H), 6.70 (s, 1 H), 6.64 (dd, J = 8.6, 1.8 Hz, 1 H). ^{13}C{H} NMR (125 MHz, CD_3OD): δ (ppm) 148.7, 143.5, 134.6, 122.2, 117.9, 114.6, 93.3.

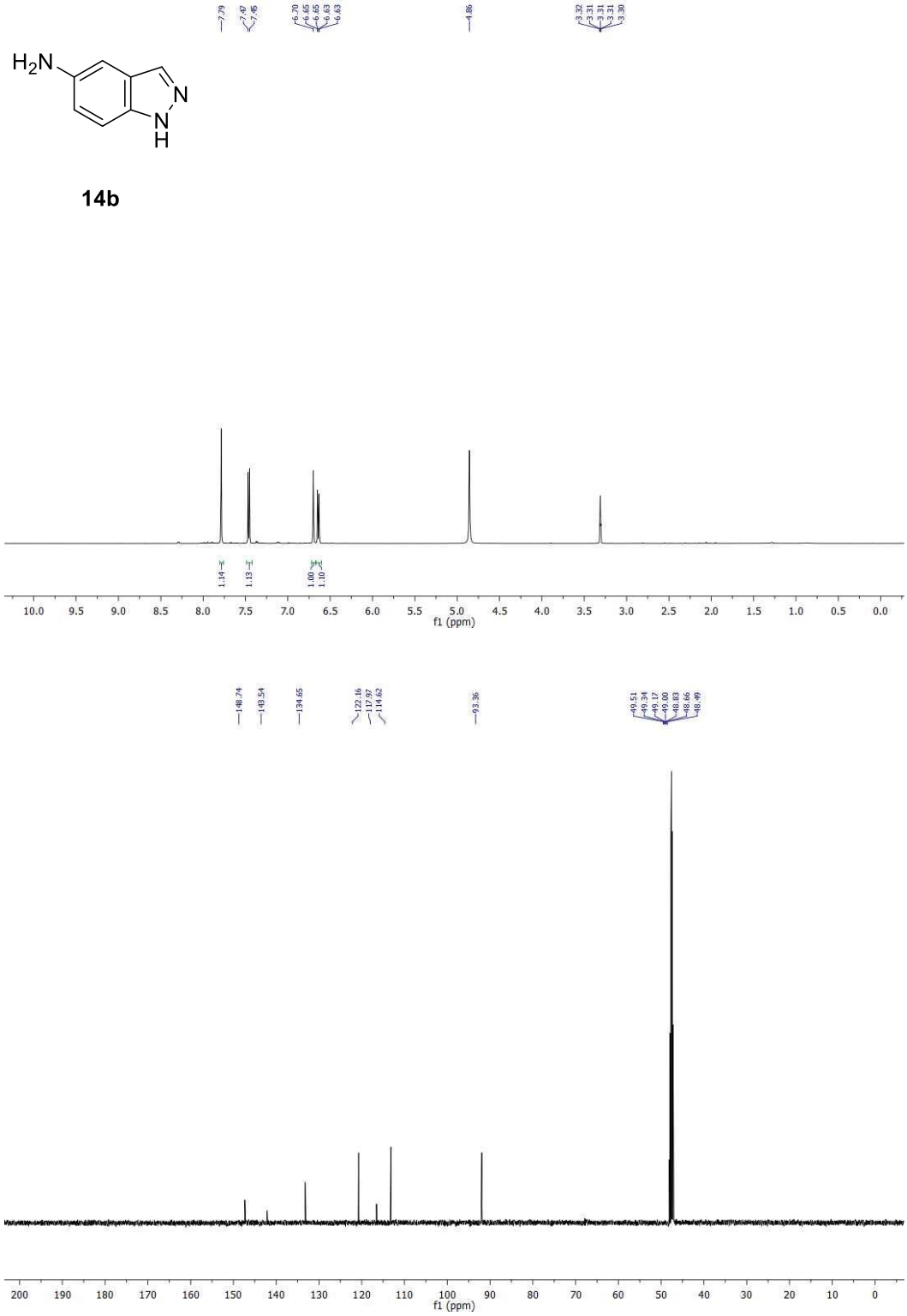

Figure S28. ^{1}H NMR (500 MHz, CD_3OD) and ^{13}C{H} NMR (125 MHz, CD_3OD) spectra of **14b**.

methyl (E)-3-(4-aminophenyl)acrylate (**16b**):[8] yellow solid, (24 mg, yield: 68%). ^{1}H NMR (500 MHz, $CDCl_3$): δ (ppm) 7.60 (d, J = 15.9 Hz, 1 H), 7.35 (d, J = 8.4 Hz, 2 H), 6.65 (d, J = 8.4 Hz, 2 H), 6.24 (d, J = 15.9 Hz, 1 H), 3.78 (s, 3 H). ^{13}C{H} NMR (125 MHz, $CDCl_3$): δ (ppm) 168.2, 148.7, 145.2, 129.9, 124.7, 114.9, 113.3, 51.5.

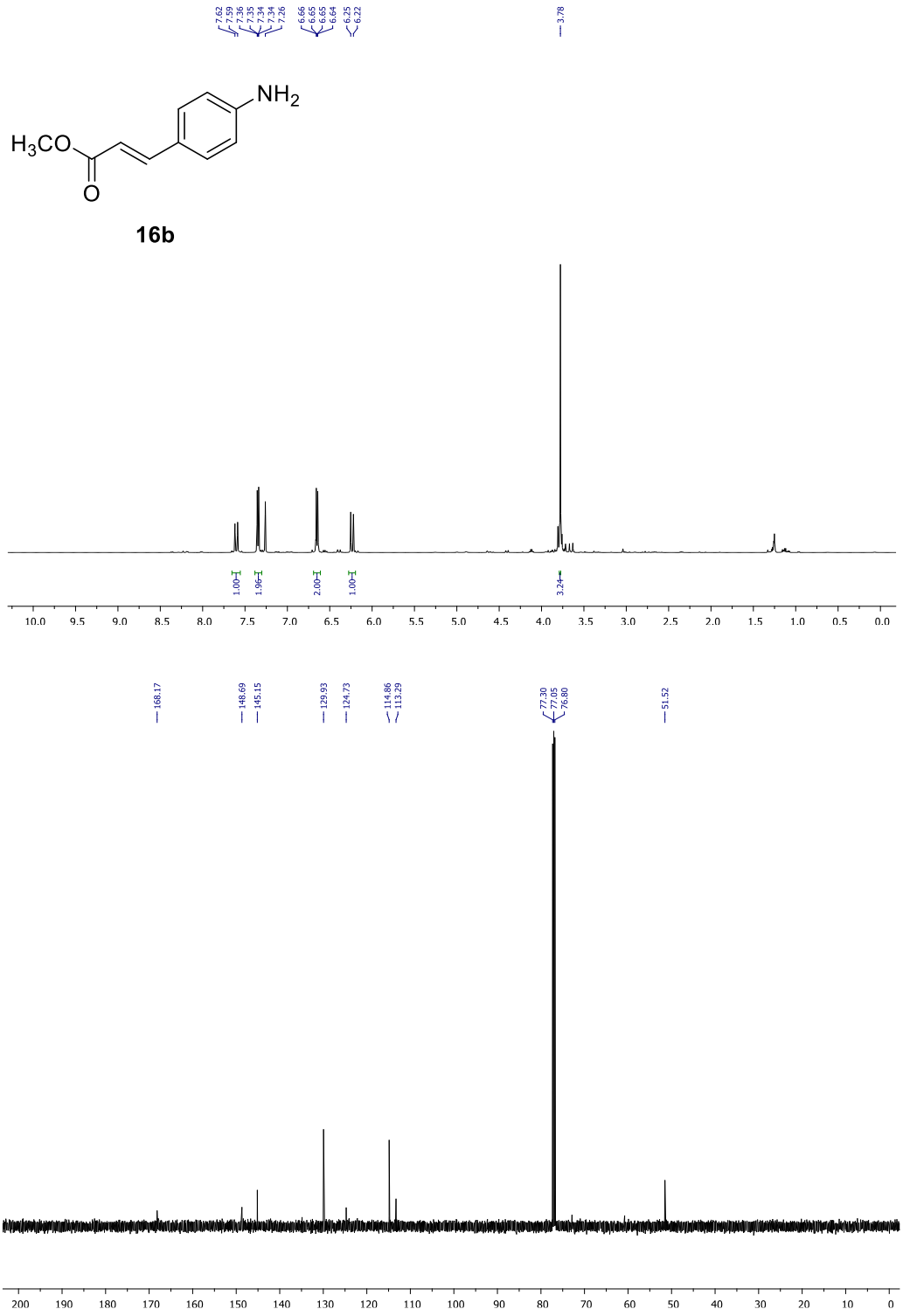

Figure S29. ^{1}H NMR (500 MHz, $CDCl_3$) and ^{13}C{H} NMR (125 MHz, $CDCl_3$) spectra of **16b**.

N-(1H-imidazol-2-yl)hydroxylamine (**17c**):[6] white solid, (16 mg, yield: 85%). ^{1}H NMR (500 MHz, CD_3OD): δ (ppm) 7.10 (s, 2 H), 4.95 (br s, 1 H). $^{13}C\{^{1}H\}$ (125 MHz, CD_3OD): δ (ppm) 136.5, 131.0 (2C).

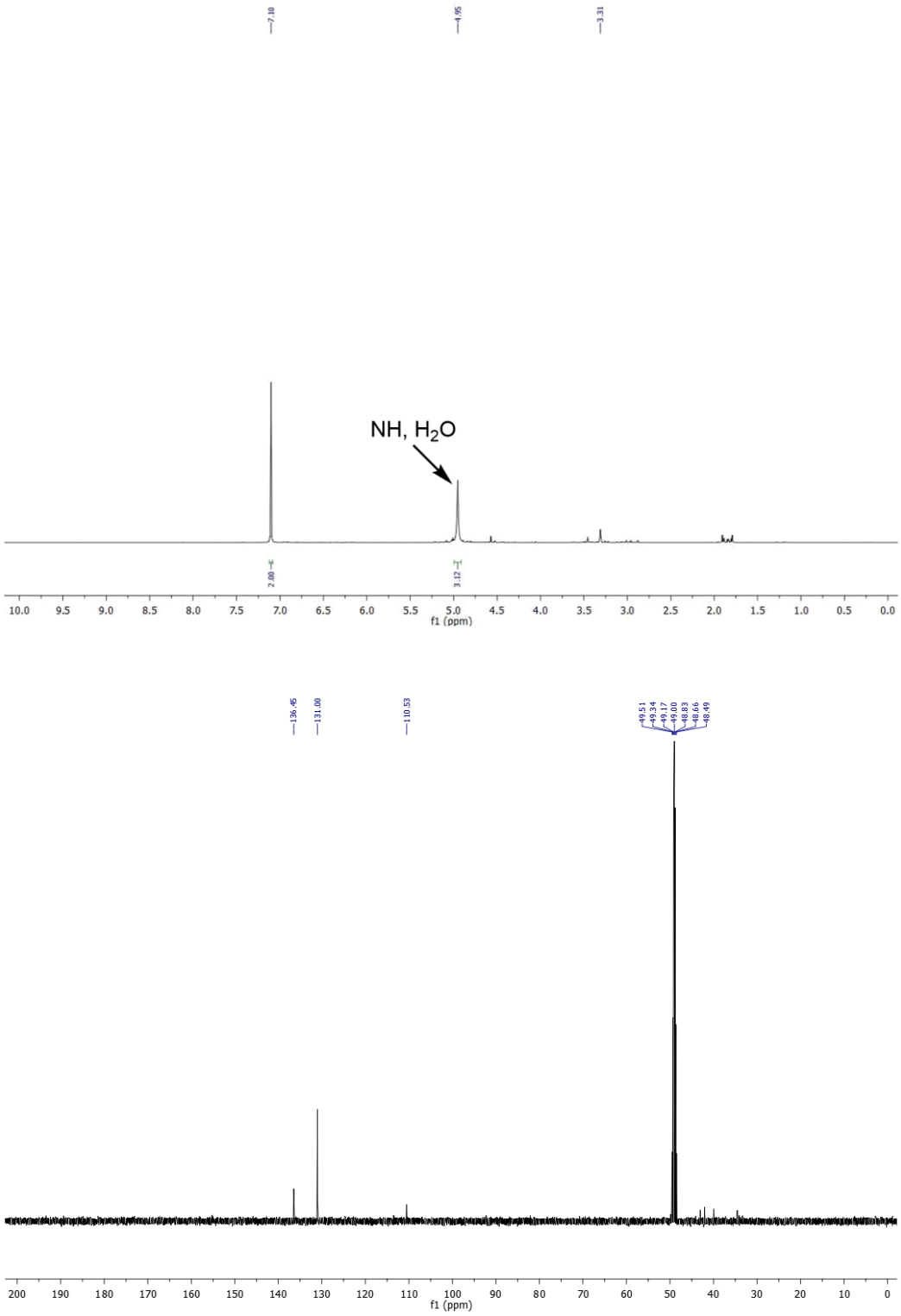

Figure S30. ^{1}H NMR (500 MHz, CD_3OD) and $^{13}C\{H\}$ NMR (125 MHz, CD_3OD) spectra of **17c**.

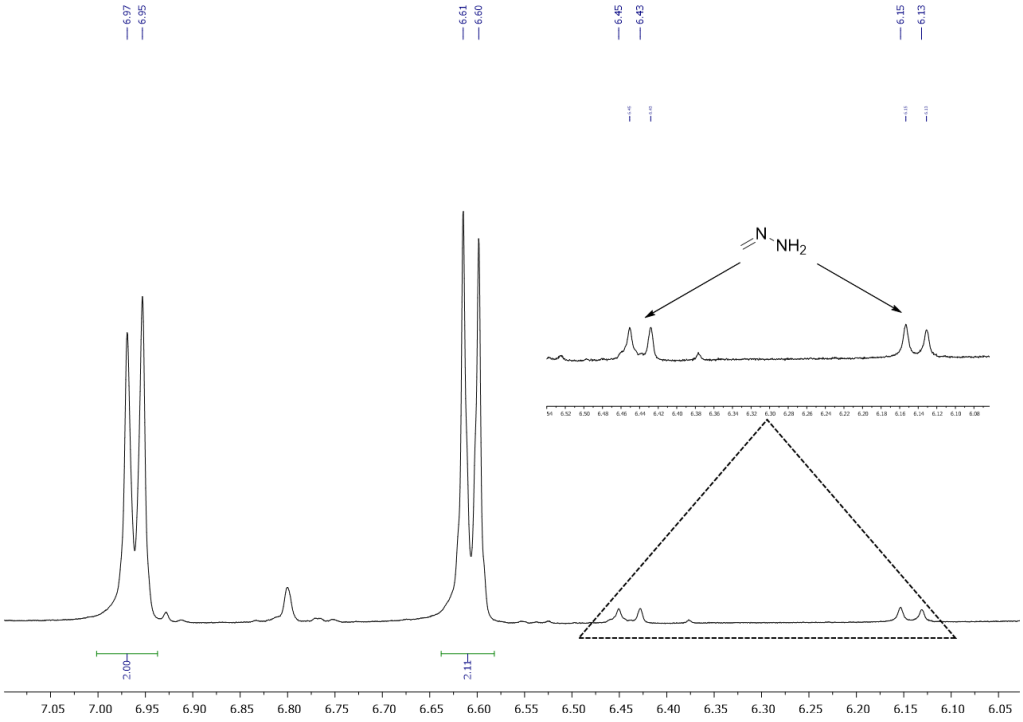

Figure S31. ^{1}H NMR (500 MHz, CD_3OD) of crude reaction mixture of the reduction of **1a** in the presence **2** and 1 equiv CH_3NHNH_2.

S2.4 Mechanistic studies

S2.4.1 High-resolution mass spectrometry

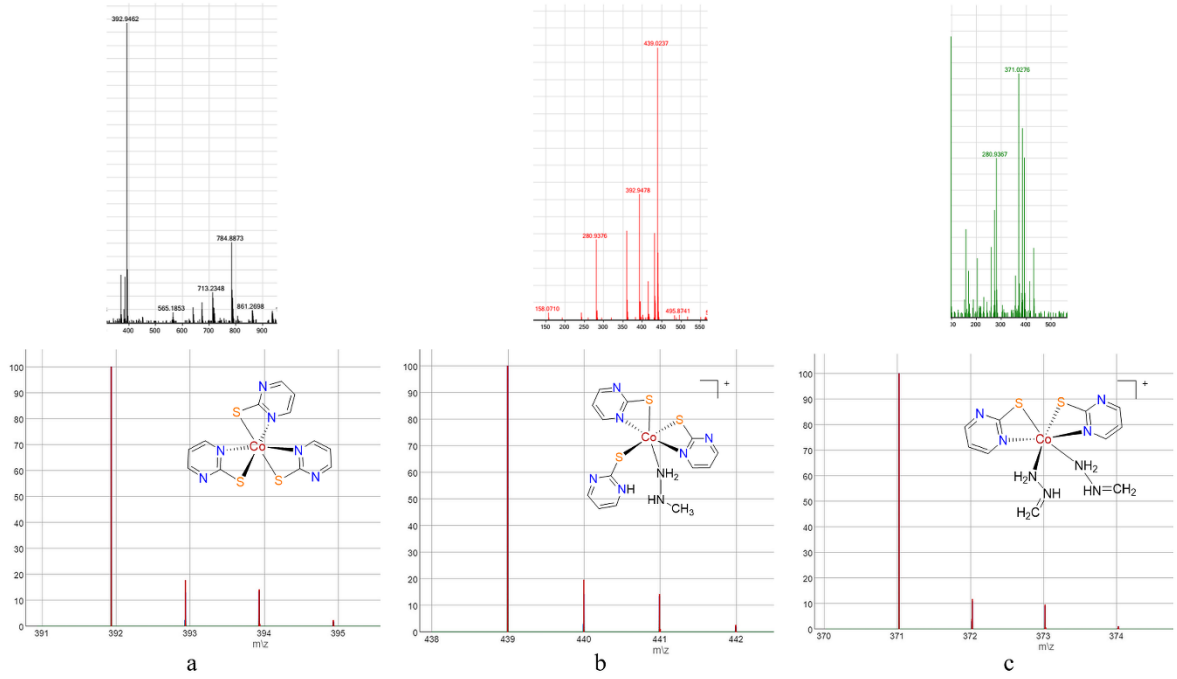

Figure S32. Upper part: High-resolution mass spectra of: (a) **1** in CH_3OH, (b) **1** in CH_3OH after addition of 1-2 equiv of CH_3NHNH_2, (c) **1** in CH_3OH after addition of more than 3 equiv of CH_3NHNH_2. Lower part: Calculated mass spectra that correspond to the observed mass peaks *m/z* and their assignments to the species (a) $[Co(pymt)_3+H]^+$, (b) $[Co(pymt)_2(pymtH)(CH_3NHNH_2)]^+$ and (c) $[Co(pymt)_2(CH_2=NNH_2)_2]^+$.

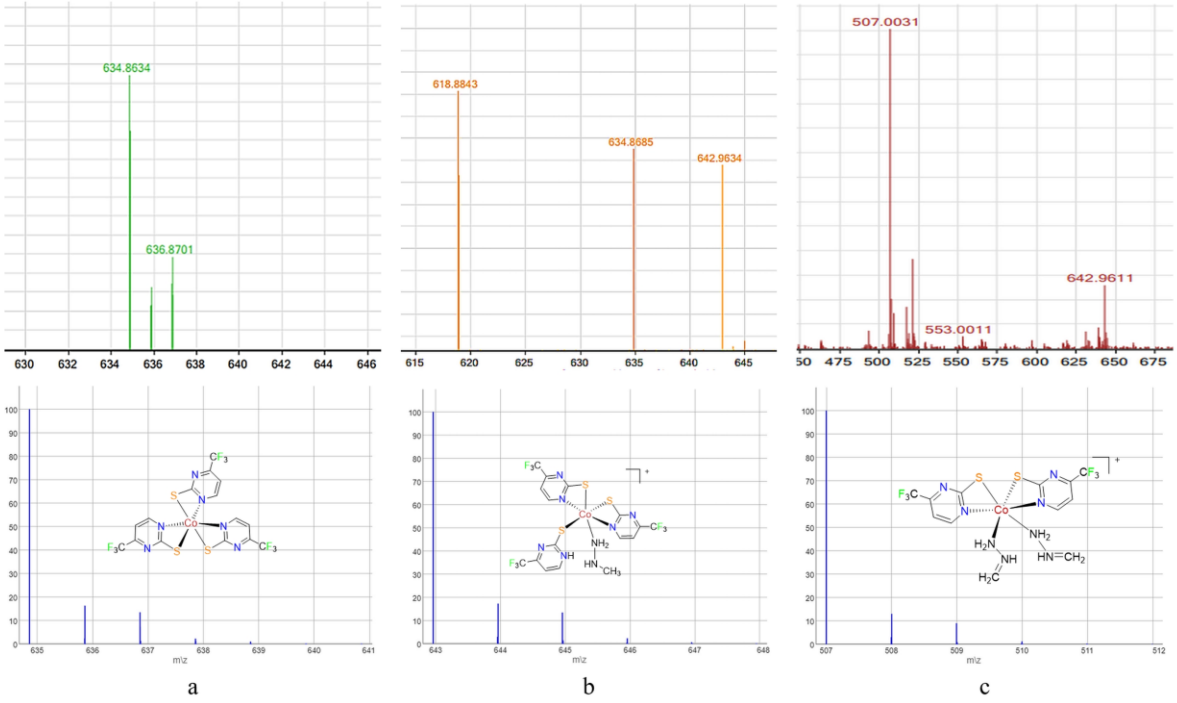

Figure S33. Upper part: High-resolution mass spectra of: (a) **2** in CH_3OH, (b) **2** in CH_3OH after addition of 1-2 equiv of CH_3NHNH_2, (c) **2** in CH_3OH after addition of more than 3 equiv of CH_3NHNH_2. Lower part: Calculated mass spectra that correspond to the observed mass peaks *m/z* and their assignments to the species (a) $[Co(tfmp2S)_3+K]^+$, (b) $[Co(tfmp2S)_2(tfmp2SH)(CH_3NHNH_2)]^+$ and (c) $[Co(tfmp2S)_2(CH_2=NNH_2)_2]^+$.

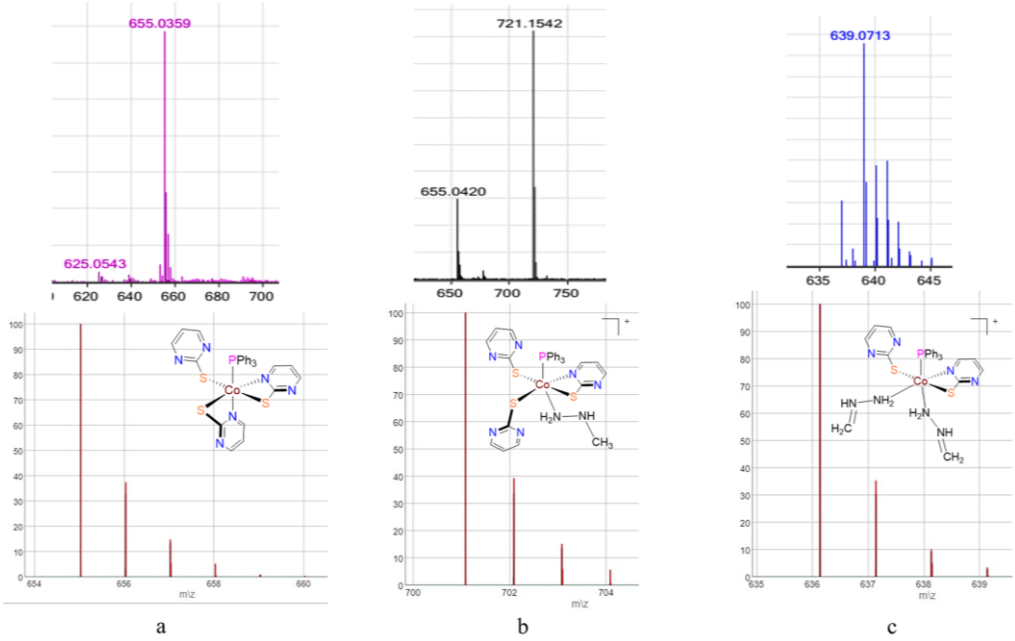

Figure S34. Upper part: High-resolution mass spectra of: (a) **5** in CH_3OH, (b) **5** in CH_3OH after addition of 1-2 equiv of CH_3NHNH_2, (c) **5** in CH_3OH after addition of more than 3 equiv of CH_3NHNH_2. Lower part: Calculated mass spectra that correspond to the observed mass peaks *m/z* and their assignments to the species (a) $[Co(pymt)_3(PPh_3)]^+$, (b) $[Co(pymt)_2(pymtH)(PPh_3)(CH_3NHNH_2)+K]^+$ and (c) $[Co(pymt)_2(pymtH)(PPh_3)(CH_2{=}NNH_2)_2]^+$.

S2.4.2 UV-vis absorption spectroscopy

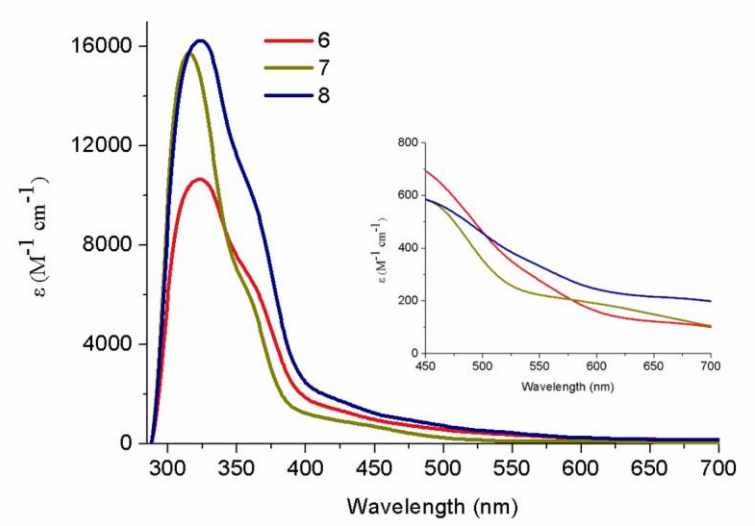

Figure S35. UV-vis absorption spectra of **6**-**8** in CH_3OH (2×10^{-4} M). Inset: UV-vis absorption spectra of the lower energy region of **6**-**8** in CH_3OH (3×10^{-3} M).

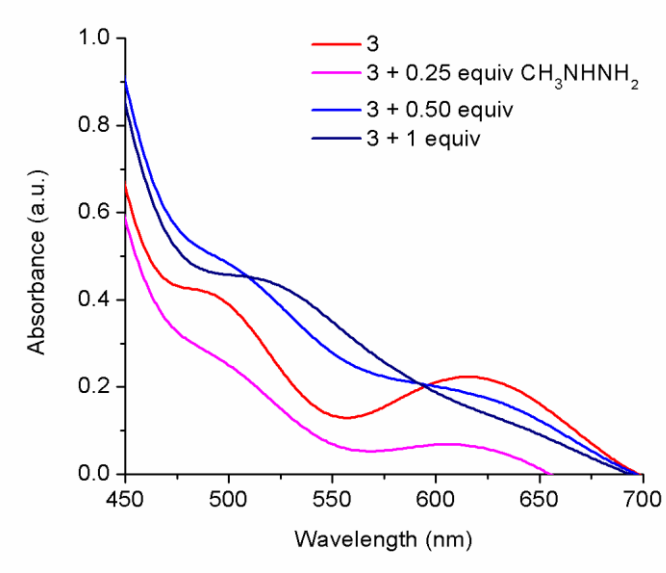

Figure S36. UV-vis absorption spectra of **3** in CH_3OH (3×10^{-3} M) upon addition of increasing amounts (0.25-1 equiv) of CH_3NHNH_2.

S2.4.3 Cyclic voltammetry

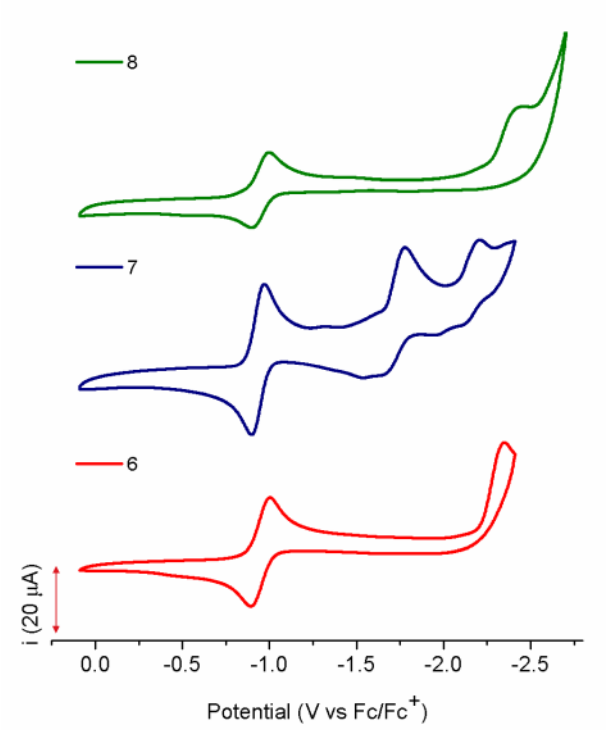

Figure S37. Cyclic voltammetry data for the pyridine-based thioamidato Co(III) complexes **6**-**8** in CH_3CN (all spectra were shifted vertically for the sake of clarity).

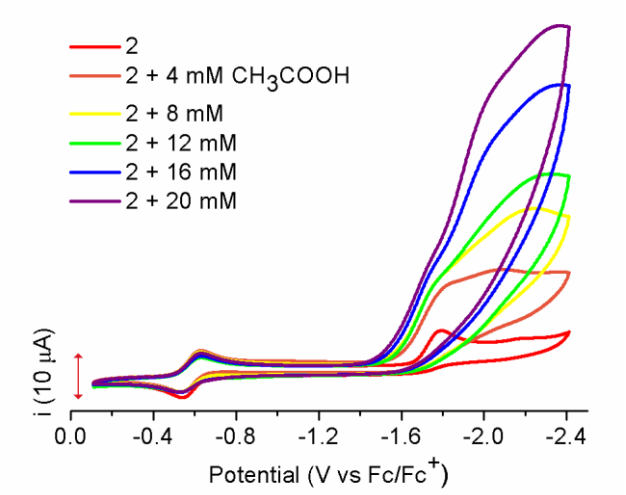

Figure S38. Cyclic voltammetry data of **2** in CH_3CN upon addition of increasing amounts of CH_3COOH.

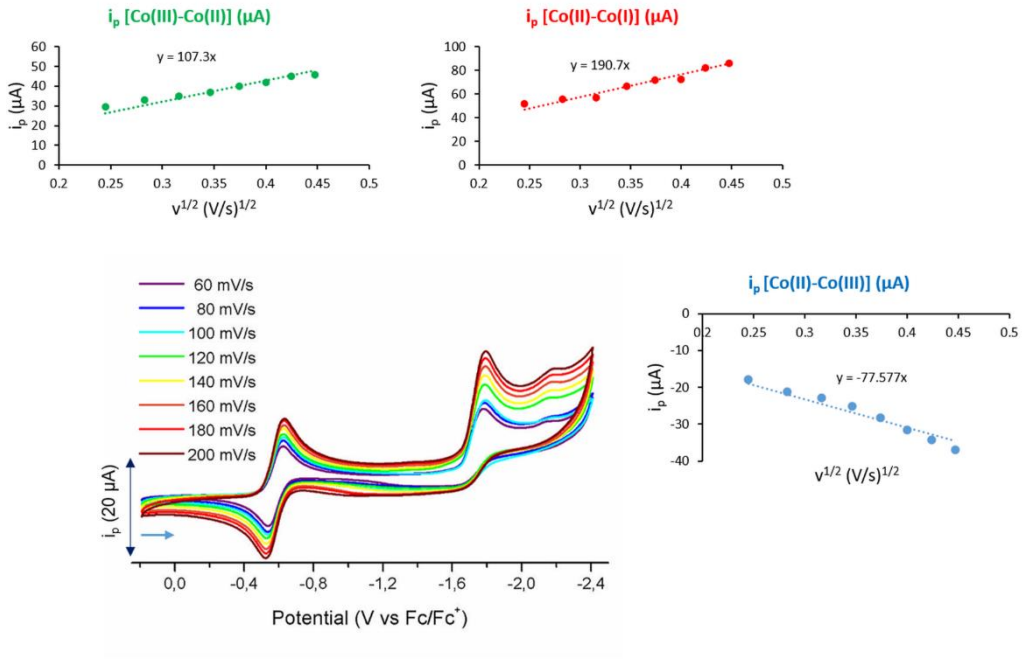

Figure S39. Left side: Overlay of cyclic voltammograms of **2** in CH_3CN at different scan rates from 60 to 200 mV. Top and right side: Peak current (I_p) vs square roots of the scan rates ($v^{1/2}$) plots for the Co(III)/Co(II), Co(II)/Co(I) and Co(II)/Co(III) redox processes.

CV measurements of **2** at different scan rates show that the peak currents (I_p) associated with both reduction processes vary linearly with the square root of the scan rates and follow the Randles-Sevcik diffusion equation, $I_p = 0.4463(F/RT)^{1/2}n_p^{3/2}FAD^{1/2}[C_o]v^{1/2}$, where I_p is the peak current, F is Faraday's constant (F = 96.485 C mol^{-1}), R is the universal gas constant (R = 8.314 J K^{-1} mol^{-1}), T is temperature (T = 300 K), n_p is the number of electrons transferred, A is the active surface area of the electrode, D is the diffusion coefficient of the complex, $[C_o]$ is the concentration of the catalyst, and v is the scan rate (V/s). The electrochemical diffusion coefficients of **2** were determined to be 8.5×10^{-6}, 22.5×10^{-6} cm^2 s^{-1} for the first and the second reduction processes, respectively (the diffusion coefficients are mentioned in anodic scan). The observation of similar slopes in the I_p *vs* $v^{1/2}$ plots for both of these processes provides an indication of the homogeneous behavior of the complex during its reduction from Co(III) to Co(I), and not the formation of nanoparticles.

S2.4.4 Gas chromatography analysis

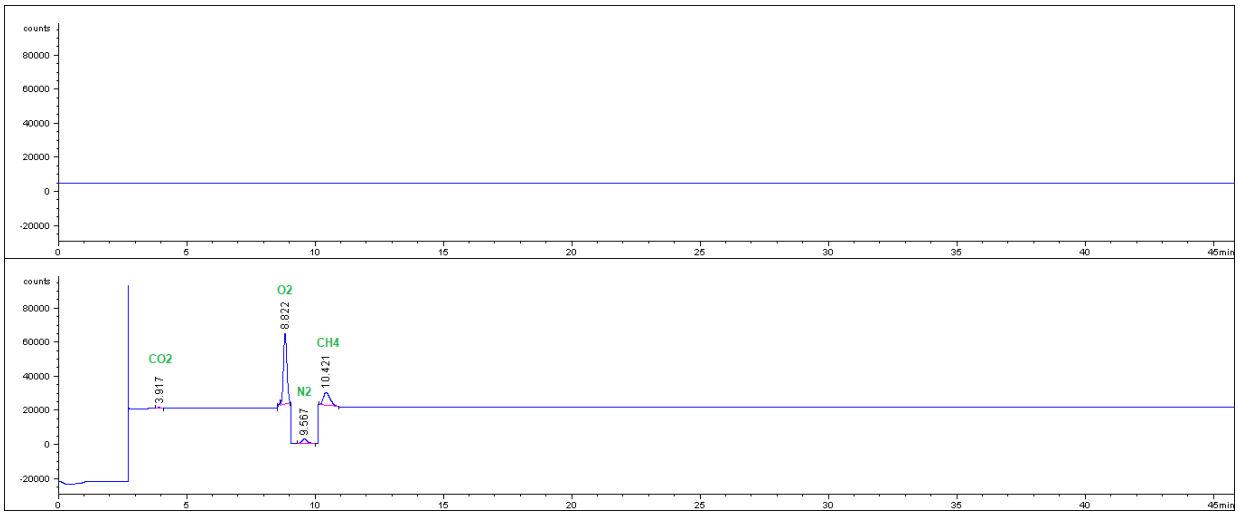

Figure S40. GC-TCD chromatogram of the reaction mixture in the presence of **2** and CH_3NHNH_2 in CH_3OH (CH_4: 2.9%, N_2: 8.6%).

REFERENCES

1 Bruker Analytical X-ray Systems, Inc., 2006. Apex2, Version 2 User Manual, M86-E01078, Madison, WI.

2 P. W. Betteridge, J. R. Carruthers, R. I. Cooper, K. Prout, D. J. Watkin, Software for guided crystal structure analysis, J. Appl. Cryst., 2003, 36, 1487.

3 C. F. Macrae, P. R. Edgington, P. McCabe, E. Pidcock, G. P. Shields, R. Taylor, M. Towler, J. van de Streek, Mercury: visualization and analysis of crystal structures, J. Appl. Cryst., 2006, **39**, 453-457.

4 E. Vasilikogiannaki, C. Gryparis, V. Kotzabasaki, I. N. Lykakis, M. Stratakis, *Adv. Synth. Catal.*, 2013, **355**, 907-911.

5 D. I. Ioannou, D. K. Gioftsidou, V. E. Tsina, M. G. Kallitsakis, A. G. Hatzidimitriou, M. A. Terzidis, P. A. Angaridis, I. N. Lykakis, *J. Org. Chem.*, 2021, **86**, 2895-2906.

6 M. G. Kallitsakis, D. I. Ioannou, M. A. Terzidis, G. E. Kostakis, I. N. Lykakis, *Org. Lett.,* 2020, **22**, 4339-4343.

7 Y. Y. See, M. S. Sanford, *Org. Lett.*, 2020, **22**, 2931-2934.

8 F. Hochberger-Roa, S. Cortés-Mendoza, D. Gallardo-Rosas, R. A. Toscano, M. C. Ortega-Alfaro, J. G. López-Cortés, *Adv. Synth. Catal*., 2019, **361**, 4055-4064.